

# 1 Regeneration following tissue necrosis is 2 mediated by non-apoptotic caspase activity

3  
4 Jacob W. Klemm, Chloe Van Hazel, Robin E. Harris

5 Arizona State University, 427 E Tyler Mall LSE 229, Tempe, AZ 85287-4501

6  
7 Corresponding author: [robin.harris@asu.edu](mailto:robin.harris@asu.edu)

8 Running title: Dronc promotes necrosis-induced regeneration.

## 9 10 Abstract

11 Tissue necrosis is a devastating complication for many human diseases and injuries.  
12 Unfortunately, our understanding of necrosis and how it impacts surrounding healthy tissue –  
13 an essential consideration when developing methods to treat such injuries – has been limited  
14 by a lack of robust genetically tractable models. Our lab previously established a method to  
15 study necrosis-induced regeneration in the *Drosophila* wing imaginal disc, which revealed a  
16 unique phenomenon whereby cells at a distance from the injury upregulate caspase activity in a  
17 process called Necrosis-induced Apoptosis (NiA) that is vital for regeneration. Here we have  
18 further investigated this phenomenon, showing that NiA is predominantly associated with the  
19 highly regenerative pouch region of the disc, shaped by genetic factors present in the  
20 presumptive hinge. Furthermore, we find that a proportion of NiA fail to undergo apoptosis,  
21 instead surviving effector caspase activation to persist within the tissue and stimulate  
22 reparative proliferation late in regeneration. This proliferation relies on the initiator caspase  
23 Dronc, and occurs independent of JNK, ROS or mitogens associated with the previously  
24 characterized Apoptosis-induced Proliferation (AiP) mechanism. These data reveal a new means  
25 by which non-apoptotic Dronc signaling promotes regenerative proliferation in response to  
26 necrotic damage.

## 27 **Introduction**

28 Necrosis is the rapid, disordered death of cells characterized by the loss of membrane integrity and release  
29 of cytoplasmic contents into the surrounding tissue (Hajibabaie *et al.* 2023). This catastrophic type of cell  
30 death can occur in diverse tissues and is central to many human conditions, particularly those related to  
31 ischemic injuries. Such conditions can include chronic illnesses like diabetes, joint disorders, sickle-cell  
32 anemia and other inherited and congenital diseases (Masi *et al.* 2007, Mulay *et al.* 2016, Karsch-Bluman *et al.*  
33 *et al.* 2019, Tonnus *et al.* 2021, Li *et al.* 2023), as well as more acute medical events like strokes, heart  
34 attacks, bacterial infections and common traumatic injuries (Konstantinidis *et al.* 2012, Hakkarainen *et al.*  
35 2014, Bonne and Kadri 2017, Wu *et al.* 2018). Even therapeutic interventions, in particular treatments for  
36 cancer, can result in this devastating form of damage (Robertson *et al.* 2017, Nakada *et al.* 2019, Yang *et al.*  
37 *et al.* 2021). Unfortunately, current strategies to treat necrosis mainly focus on invasive procedures that are  
38 often met with limited success. With such substantial bearings on human health, it is crucial to better  
39 understand the effects of necrosis in disease and injury, particularly in the context of tissue repair and  
40 regeneration.

41 Unfortunately, we currently have a limited understanding of how necrosis impacts surrounding healthy tissue  
42 during wound healing. Indeed, much of our understanding about how cell death influences tissue repair  
43 comes instead from models involving programmed cell death (PCD) like apoptosis (Hajibabaie *et al.* 2023).  
44 This highly regulated process can be triggered by intrinsic or extrinsic pathways, both of which lead to the  
45 activation of caspases that mediate the controlled disassembly of the cell (Ashkenazi and Salvesen 2014).  
46 Studies of PCD in a variety of species have shown that cells undergoing apoptosis can release signaling  
47 molecules that are interpreted by surrounding tissues to drive wound healing events, such as tissue  
48 remodeling, immune responses, survival and proliferation of surrounding cells (Tseng *et al.* 2007, Fan and  
49 Bergmann 2008, Chera *et al.* 2009, Bergmann and Steller 2010, Li *et al.* 2010, Pellettieri *et al.* 2010, Ryoo  
50 and Bergmann 2012, Vriza *et al.* 2014, Fuchs and Steller 2015, Perez-Garijo and Steller 2015, Fogarty and  
51 Bergmann 2017, Perez-Garijo 2018). For example, the signaling molecules Prostaglandin E2 and Hedgehog  
52 are produced by dying hepatocytes to induce regenerative proliferation in the vertebrate liver (Jung *et al.*  
53 2010, Li *et al.* 2010), while apoptotic-deficient mice show both impaired liver regeneration and epidermal  
54 recovery after wounding (Li *et al.* 2010). While mitogenic signaling by apoptotic cells is an established and  
55 conserved process, whether similar signaling events occur following necrotic cell death is less clear.

56 Evidence of apoptotic signaling first originated from studies of the larval wing primordia in *Drosophila* (Perez-  
57 Garijo *et al.* 2004, Ryoo *et al.* 2004). This epithelial tissue has been extensively characterized as a model for  
58 growth, development and regeneration, including the role that cell death plays in these processes (Beira and  
59 Paro 2016, Worley and Hariharan 2022). Ongoing studies of this model have identified an essential  
60 signaling network centered on the highly conserved JNK pathway. JNK activates several major signaling

61 pathways including Hippo and JAK/STAT, which have conserved roles in promoting regeneration across  
62 species (Worley *et al.* 2012, Hariharan and Serras 2017, Fox *et al.* 2020, Worley and Hariharan 2022), as  
63 well as activating JNK itself via overlapping feed-forward loops. One such feed-forward mechanism acts  
64 through the initiator caspase Dronc (*Drosophila* Caspase-9), which, independent of its role in apoptosis, is  
65 translocated to the cell membrane to activate the release of ROS from the NADPH oxidase Duox  
66 (Amcheslavsky *et al.* 2018). ROS attracts hemocytes to further activate JNK signaling in the disc through the  
67 release of the TNF ligand Eiger (Fogarty *et al.* 2016, Diwanji and Bergmann 2018). In a related pathway,  
68 JNK can also lead to the expression of the *Duox* maturation factor *moladietz* (*mol*), thus activating this loop  
69 without Dronc (Khan *et al.* 2017, Pinal *et al.* 2018). An important advance in elucidating this network was the  
70 ability to generate “undead cells”, using the baculovirus caspase inhibitor P35 to prevent apoptotic cells from  
71 dying (Hay *et al.* 1994). These cells therefore persist, releasing mitogenic factors including Wingless (Wg,  
72 Wnt1), Decapentaplegic (Dpp, BMP2/4), Spitz (Spi, EGF) or Hedgehog (Hh) (Huh *et al.* 2004, Perez-Garijo  
73 *et al.* 2004, Ryoo *et al.* 2004, Perez-Garijo *et al.* 2005, Fan and Bergmann 2008, Perez-Garijo *et al.* 2009,  
74 Morata *et al.* 2011, Fan *et al.* 2014). These signals subsequently promote proliferation of the surrounding  
75 cells in a phenomenon known as Apoptosis-induced Proliferation (AiP) (Fan and Bergmann 2008, Ryoo and  
76 Bergmann 2012, Fogarty and Bergmann 2017).

77 By contrast, the genetic events following necrosis are less well explored. Necrosis is characterized by  
78 swelling and loss of cellular membrane integrity, with the release of cellular contents into the intercellular  
79 space causing a significant inflammatory response (Festjens *et al.* 2006, D'Arcy 2019, Hajibabaie *et al.*  
80 2023). Necrosis is highly variable, occurring as a regulated process, for example necroptosis, or as  
81 unregulated, caspase-independent cell lysis (Ashkenazi and Salvesen 2014, D'Arcy 2019). The factors  
82 released from necrotic cells are collectively termed Damage-Associated Molecular Patterns  
83 (DAMPs)(Venereau *et al.* 2015, Roh and Sohn 2018), which are thought to interact with pattern recognition  
84 receptors (PRRs) on nearby cells, mostly of the Toll-like receptor (TLR) family (Ming *et al.* 2014, Gong *et al.*  
85 2020). DAMPs are understood to mainly consist of fundamental cellular components like histones,  
86 chromatin, and actin (Venereau *et al.* 2015, Gordon *et al.* 2018, Roh and Sohn 2018), although specific  
87 factors have been also been described. For example, High-mobility group box 1 (HMBG1) has been  
88 characterized as a DAMP in models of spinal cord, cardiac and muscle injury where it promotes  
89 angiogenesis, attracts repair cells and induces proliferation (Venereau *et al.* 2015), as well as in *Drosophila*  
90 models of necrosis (Nishida *et al.* 2024). However, the overall role of DAMPs and how they influence healing  
91 and regeneration through interaction with healthy tissues has yet to be fully explored.

92 To investigate necrosis-induced wound repair and regeneration, our lab developed a method to rapidly and  
93 reproducibly induce necrotic cell death within the developing *Drosophila* wing imaginal discs (Klemm *et al.*  
94 2021). Using a genetic ablation system we previously established, named Duration and Location (DUAL)  
95 Control (Harris 2023), we can induce necrosis in the wing disc via expression of a leaky cation channel

96 *GluR1<sup>LC</sup>* (Liu *et al.* 2013, Yang *et al.* 2013). Using this system (*DC<sup>GluR1</sup>*), we showed that wing discs are  
97 capable of fully regenerating following necrotic injury at a level comparable to that of damage induced by  
98 apoptosis (Klemm *et al.* 2021). However, while apoptotic ablation leads to JNK signaling and extensive  
99 caspase activity, we found that necrosis leads to only a minor level of JNK-mediated apoptosis, which is  
100 confined to the wound edge, but unexpectedly generates significant caspase activity in cells distant from the  
101 injury. We called this non-autonomous caspase activation Necrosis-induced Apoptosis (NiA) (Klemm *et al.*  
102 2021). Unlike normal apoptotic cells, NiA form entirely independent of JNK signaling, and cannot be made  
103 undead using P35. We also demonstrated that NiA is essential for regeneration, although how was unclear.  
104 Here we have further characterized the NiA phenomenon, finding that only regeneration-competent areas of  
105 the wing disc can produce NiA following damage, in part due to WNT and JAK/STAT signaling in the hinge  
106 that limits NiA to the pouch. Building upon our finding that NiA is necessary for regeneration, we show that  
107 NiA leads to localized proliferation significantly later in regeneration than previously appreciated. Using tools  
108 to trace caspase activity and cell death, we demonstrate that this is possible because a proportion of NiA  
109 survive effector caspase activation and persist late into regeneration where they promote proliferation.  
110 Finally, we show that this proliferation relies on the initiator caspase Dronc, but surprisingly does not involve  
111 established AiP mechanisms. Our data suggest a model in which necrotic injuries induce caspase activity in  
112 cells at a distance from the injury, some of which undergo JNK-independent apoptosis (NiA), while others  
113 survive and promote proliferation through a novel non-apoptotic function of Dronc, which is separate from its  
114 role in AiP. We refer to these surviving NiA cells as Necrosis-induced Caspase-Positive (NiCP) cells. These  
115 findings reveal an important genetic response to lytic cell death that could potentially be leveraged to  
116 augment regeneration of necrotic wounds.

117

## 118 **Results**

### 119 **Formation of NiA occurs primarily in the wing pouch.**

120 Previously, we found that NiA occurs in the lateral pouch (LP) upon induction of necrosis in the distal pouch  
121 with *DC<sup>GluR1</sup>* (Figure 1A, D and E, yellow arrowheads in E) (Klemm *et al.* 2021). The wing disc itself  
122 comprises different identities reflecting the adult structures they ultimately create, including the pouch, hinge  
123 and notum, which are themselves divided into compartments; anterior/posterior and dorsal/ventral (Figure  
124 1B). Since these various disc identities have distinct regenerative capacities stemming from their different  
125 genetic responses to damage (Martin *et al.* 2017), to better understand the formation of NiA and the role it  
126 plays in regeneration, we tested whether necrosis occurring in different areas of the disc leads to NiA. To do  
127 so, we utilized *GAL4/UAS/GAL80<sup>ts</sup>* to conditionally express *UAS-GluR1<sup>LC</sup>* in the pouch, hinge or notum  
128 tissues (Figure 1B and C) (Yang *et al.* 2013). As an initial test, we attempted to recapitulate our original  
129 observations made using *DC<sup>GluR1</sup>* by employing an enhancer of the *spalt* gene driving *GAL4*

130 (*R85E08<sup>ts</sup>>GluR1*) to cause necrosis in the distal pouch (Figure 1F and G). As anticipated, NiA are formed  
131 in the LP following 20 hr of ablation (denoted as 0 hr, when larvae are downshifted to 18°C) (Figure 1G). In  
132 this figure and others, NiA are recognized as cells positive for the cleaved caspase Dcp-1 and negative for  
133 GFP that labels the ablation domain (*UAS-GFP*) (Figure 1E and G, yellow arrowheads), which indicates that  
134 these caspase-positive cells originate outside the area of ablation. This test confirms that the NiA  
135 phenomenon occurs independent of the ablation system used. Notably, NiA are consistently absent from the  
136 presumptive hinge region surrounding the pouch following both *R85E08<sup>ts</sup>>GluR1* or *DC<sup>GluR1</sup>* ablation (Figure  
137 1E and G). Indeed, outside of the pouch, Dcp-1 is only observed in a small area of the posterior pleura  
138 (Figure 1E, red arrowhead) and at low levels stochastically across the disc resulting from temperature  
139 changes (Klemm *et al.* 2021). To further investigate the extent to which necrotic pouch tissue can induce  
140 NiA we next ablated the entire pouch using *rotund-GAL4 (rn<sup>ts</sup>>GluR1)* or *nubbin-GAL4 (nub<sup>ts</sup>>GluR1)*  
141 (Figure 1H, I and J, figure 1- figure supplement 1A). Necrosis of the whole pouch with either driver results in  
142 significant Dcp-1 (Figure 1I and Figure 1 – figure supplement 1A). However, the majority of these cells also  
143 have GFP and frequently overlap with expression of the JNK target *Mmp1* (Figure 1I and J), therefore  
144 resembling cells undergoing JNK-mediate apoptosis, such as those at the wound edge (WE) following distal  
145 pouch ablation (Figure 1 – figure supplement 1B, arrowhead), rather than NiA (Klemm *et al.* 2021)). These  
146 data suggest that cells outside of the pouch are generally unable to respond to DAMPs released by pouch  
147 cells undergoing necrosis to generate NiA, or that such DAMPs are spatially limited.

148 To test whether necrosis in areas outside of the pouch can induce NiA, we ablated the proximal notum using  
149 *pannier-GAL4 (pnr<sup>ts</sup>>GluR1)* (Figure 1K), using the absence of the notum Wg stripe to confirm loss of this  
150 area (Figure 1L and M, open arrowheads). We observed only minimal NiA, with sporadic Dcp-1-positive,  
151 GFP-negative cells in the unablated areas of the notum (Figure 1L), which remains unchanged after 24 hr  
152 (Figure 1M). To test the hinge, we used a putative *zfh1* enhancer driving *GAL4 (R73G07<sup>ts</sup>>GluR1)*, which  
153 has hinge-specific expression (Figure 1N). Ablation of the hinge fails to generate NiA in the notum, but  
154 surprisingly does not induce a response in the neighboring pouch cells (Figure 1O and P, open arrowhead in  
155 O), despite their demonstrated ability to form NiA (Figure 1G). Together, these data suggest that only the  
156 pouch releases DAMPs - and has the requisite PRRs to respond to these DAMPs - that lead to NiA following  
157 necrosis.

158 As the efficacy of DAMPs might be limited by how far they can reach after being released from lysed cells,  
159 we also induced necrosis in the entire posterior disc compartment with *hedgehog-GAL4 (hh<sup>ts</sup>>GluR1)*  
160 (Figure 1Q), and in an anterior stripe along the anterior/posterior compartment boundary using *patched-*  
161 *GAL4 (ptc<sup>ts</sup>>GluR1)* (Figure 1 – figure supplement 1C). These experiments cause the simultaneous necrosis  
162 of pouch, hinge and notum tissues, allowing us to determine the potential of these different tissue identities  
163 to produce NiA. In both experiments, NiA cells are observed in the pouch, and to a lesser extent the notum,  
164 but are still strikingly absent from the hinge (Figure 1R, R' and T, Figure 1 – figure supplement 1D, D' and

165 F). After 24 hr of recovery, there is an increase in the number of NiA within the pouch and notum, but not the  
166 hinge (Figure 1S, S' and T, Figure 1 – figure supplement 1E, E' and F). Thus, it appears that NiA can occur  
167 outside of the pouch when a large enough area, or an area that also includes the pouch, is ablated.  
168 However, the hinge is refractory to NiA formation.

169 To avoid any bias in the use of tissue-specific *GAL4* drivers, we also made RFP-labeled stochastic clones  
170 that have the potential to undergo necrosis upon changing the growth temperature to 30°C (Figure 1 – figure  
171 supplement 1G). After allowing these clones to develop, we triggered necrosis in early third larval instar and  
172 examined the extent of active caspase in the different disc regions (Figure 1 – figure supplement 1H). As  
173 expected, necrosis of clones in the pouch leads to active caspases both within and surrounding the ablated  
174 area, including cells without the RFP clone label, suggesting that NiA has occurred (Figure 1 – figure  
175 supplement 1H', arrowheads). We also found that necrosis in the notum leads to comparatively little  
176 caspase labeling (Figure 1 – figure supplement 1H'') consistent with the notum being less able to generate  
177 NiA. Necrotic clones in the hinge also produces caspase activity, but most of these cells also have RFP,  
178 suggesting again that NiA does not occur in the hinge (Figure 1 – figure supplement 1H'). Notably, the use  
179 of clones that naturally vary in size also demonstrates that the area of ablation is related to the amount of  
180 NiA produced (Figure 1 – figure supplement 1I), a trend also seen with the tissue-specific ablation  
181 experiments (Figure 1 – figure supplement 1I).

182 Together, these data infer three important conclusions: 1) all areas of the disc can be killed by necrosis and  
183 therefore potentially can release DAMPs, 2) NiA is limited to the pouch when local necrosis occurs, but  
184 when multiple (or large) areas of the disc are killed, limited NiA can also be induced in the notum, although  
185 we cannot rule out that this is due to DAMPs from dying pouch cells, and 3) the hinge is refractory to NiA,  
186 which is consistent with other findings that show its resistance to apoptosis in response to irradiation  
187 (Verghese and Su 2016). Thus, the overall pattern of competence to undergo NiA appears to reflect the  
188 uneven regenerative capacity of the wing disc, with NiA formation predominantly associated with the highly  
189 regenerative wing pouch.

190

### 191 **NiA is regulated by WNT and JAK/STAT signaling.**

192 As NiA readily occurs in the pouch but is excluded from the nearby hinge, we used this contrasting response  
193 to identify genetic factors that might regulate NiA formation. The wing hinge is specified by JAK/STAT  
194 signaling during disc development, which can protect cells from irradiation-induced apoptosis potentially via  
195 the expression of *Zn finger homeodomain 2 (zfh2)* (La Fortezza *et al.* 2016, Verghese and Su 2016,  
196 Verghese and Su 2018). Alongside JAK/STAT, the presence of Wingless (*Wg*, *Drosophila Wnt1*), which  
197 encircles the pouch, may also protect cells from death and permit regeneration of the pouch through the

198 repression of *reaper* (*rpr*) (Verghese and Su 2016). As such, we investigated both JAK/STAT and Wg to  
199 determine whether they regulate NiA formation.

200 The activity of the JAK/STAT pathway can be visualized in the hinge of early third instar larval discs by a  
201 *10XSTAT-GFP* reporter (Bach *et al.* 2007)(Figure 2A). Upon ablation of the distal pouch with  $DC^{GluR1}$ , a high  
202 level of JAK/STAT activity is observed at the immediate WE (Figure 2B, arrowhead), similar to its  
203 upregulation following irradiation or apoptotic ablation (Herrera and Bach 2019). As JNK signaling is induced  
204 at the WE (Figure 1 – figure supplement 1B) (Klemm *et al.* 2021), and the *unpaired* ligands are targets of  
205 JNK signaling (Katsuyama *et al.* 2015, Jaiswal *et al.* 2023), this JAK/STAT activity is likely to be JNK-  
206 mediated. By contrast, much lower levels of JAK/STAT activity are observed in the areas of the pouch where  
207 NiA occurs (Figure 2B, open arrowheads), surrounded by the higher developmental JAK/STAT in the hinge  
208 (Figure 2B). To determine if low JAK/STAT activity is important for NiA, we knocked down the receptor  
209 *domeless* ( $UAS-dome^{RNAi}$ ) in the pouch, which results in a significant increase in NiA (Figure 2C, D and E),  
210 suggesting that JAK/STAT signaling may negatively regulate the formation of NiA. To further test this idea,  
211 we ectopically activated JAK/STAT ( $UAS-hop48A$ ). However, even in the absence of damage, this  
212 expression results in high levels of caspase positive cells (Figure 2 – figure supplement 1A and B), making it  
213 difficult to determine an effect on NiA formation. Therefore, to further investigate if JAK/STAT regulates NiA  
214 formation, we asked whether reducing developmental JAK/STAT in the hinge might lead to NiA spreading  
215 further into this region. We generated a version of DUAL Control that expresses *GAL4* in the posterior  
216 compartment by replacing the pouch-specific  $DVE \gg GAL4$  with *hh-GAL4* (Figure 2F and G, Figure 2 – figure  
217 supplement 1C). To prevent *hh-GAL4* from being active throughout development, we included  $GAL80^{ts}$   
218 (hereafter  $DC^{GluR1} hh^{ts}$ ) and used temperature changes to limit *GAL4* activity to the period just prior to  
219 ablation (Figure 2F). With this system, we knocked down the expression of the JAK/STAT transcription  
220 factor *Stat92E* ( $UAS-Stat92E^{RNAi}$ ) in the posterior compartment and ablated the distal pouch, which again  
221 shows an increase in caspase-positive cells in the pouch (Figure 2I, arrowhead), but surprisingly NiA cells  
222 are still not observed in the hinge (Figure 2I, open arrowhead). To confirm this result, we also targeted *zinc*  
223 *finger homeodomain 2* (*Zfh2*), a downstream target of the JAK/STAT pathway that potentially protects cells  
224 from apoptosis (La Fortezza *et al.* 2016, Verghese and Su 2018). The knockdown of *Zfh2* also does not  
225 result in any hinge-specific NiA formation, although an increase in pouch NiA was again observed (Figure 2  
226 – figure supplement 1E). Knockdown of *Stat92E* or *Zfh2* under non-ablating conditions does not yield any  
227 increase in caspase signal (Figure 2H, Figure 2 – figure supplement 1D). Thus, JAK/STAT signaling appear  
228 to limit NiA formation in the pouch, while the inability for NiA to expand into the hinge upon reducing  
229 JAK/STAT suggests that other hinge-specific factors may be involved.

230 Wg has also been shown to protect cells from apoptosis in the hinge (Verghese and Su 2016), and therefore  
231 could influence the formation of NiA. Unlike the stochastic heat shock-induced apoptosis (Figure 2J), we  
232 noted that NiA in the pouch frequently occurs in discrete populations that avoid Wg at the margin stripe and

233 the inner Wg circle at the boundary of the pouch and hinge (Figure 2K), limiting formation of the NiA cells to  
234 regions that appear to overlap the *vestigial quadrant enhancer* (*vgQE-lacZ*, Figure 2 – figure supplement 1F  
235 and G) (Kim *et al.* 1996). By contrast, Dcp-1-positive cells at the WE do not avoid the Wg margin stripe  
236 (Figure 2K, arrowhead), suggesting that this behavior may be specific to NiA. To test this, we utilized  
237  $DC^{GluR1} hh^{ts}$  to knock down *wg* in the posterior compartment of the disc ( $UAS-wg^{RNAi}$ ) and found that NiA now  
238 occurs in areas of the pouch where *wg* expression is lost, including the wing margin and inner hinge (Figure  
239 2M, arrowhead), unlike NiA in the anterior (Figure 2M, open arrowhead). The increase in Dcp-1-positive  
240 cells does not occur when *wg* signaling is similarly blocked without damage (Figure 2L). Notably, the  
241 converse experiment in which *wg* is ectopically expressed during ablation does not suppress NiA (Figure 2 –  
242 figure supplement 1H and I), consistent with our hypothesis that other factors, such as targets downstream  
243 of JAK/STAT, might act alongside Wg to regulate NiA. Together, these data demonstrate that both WNT and  
244 JAK/STAT signaling act to limit NiA, thus potentially constraining it to the pouch following necrosis.

245

#### 246 **NiA promotes proliferation late in regeneration.**

247 As NiA is spatially regulated by at least two major signaling pathways in the disc, we next focused on how  
248 the localization of NiA relates to its role in promoting regeneration. In our previous work, using an E2F  
249 reporter (*PCNA-GFP*) we found that the appearance of NiA coincides with an uptick in proliferation at 18 hr  
250 post-ablation close to the wound, which persists at 24 hr post ablation (Klemm *et al.* 2021). However, our  
251 investigation at subsequent time points of recovery shows that regenerative proliferation continues to  
252 increase through 36 hr and 48 hr of regeneration, later than initially assayed (Figure 3A-A'''). To quantify this  
253 proliferation, we used EdU to assay the relative level of cell proliferation in discs throughout regeneration  
254 from 18 hr to 48 hr post-ablation with  $DC^{GluR1}$  (Figure 3B-B'''), using folds as landmarks to normalize EdU  
255 intensity in the pouch relative to the disc (Figure 3 – figure supplement 1A-A'''). We also performed the same  
256 time course with apoptotic ablation using  $DC^{hepCA}$  for comparison (Figure 3C-C'''). At 18 hr of regeneration  
257 following ablation with either  $DC^{GluR1}$  or  $DC^{hepCA}$ , cells at the WE have already migrated distally to close the  
258 injury, while EdU is absent from an area immediately adjacent to the wound (Figure 3B and C). This is  
259 consistent with the recently described JNK-mediated pause in proliferation that occurs in regenerating wing  
260 discs (Jaiswal *et al.* 2023). At 24 hr, this proliferation-devoid area continues to persist following apoptotic  
261 injury ( $DC^{hepCA}$ ) and the EdU signal becomes elevated broadly across the rest of the pouch, representing the  
262 formation of a blastema (Figure 3C'). By contrast, at 24 hr after necrosis ( $DC^{GluR1}$ ), the EdU label is  
263 reestablished in cells around the wound showing that proliferation has restarted in these cells (Figure 3B').  
264 Unlike  $DC^{hepCA}$ , the rest of the pouch does not appear to change its rate of proliferation (Figure 3B'). By 36  
265 hr following necrosis, an intense uptick in EdU occurs broadly across the pouch, which is significantly  
266 stronger compared to discs ablated by apoptosis (Figure 3B'', C'' and E). This increase is maintained at 48  
267 hr and remains consistently higher in  $DC^{GluR1}$  versus  $DC^{hepCA}$  ablated discs (Figure 3B''', C''' and E). Thus,

268 the timeline of recovery from necrosis appears to be distinct from that of apoptotic injury, with the strongest  
269 increases in regenerative proliferation occurring at comparatively later stages.

270 These observed increases in proliferation at 36 hr occur after the appearance of NiA. We previously showed  
271 that blocking the apoptotic pathway by simultaneously knocking down DIAP1 inhibitors *rpr*, *hid* and *grim*  
272 (*UAS-mir(RHG)*, (Siegrist *et al.* 2010) throughout the pouch limits the initial uptick in proliferation at early  
273 stages (18 – 24 hr) and inhibits regeneration (Klemm *et al.* 2021). However, it remains unclear whether this  
274 newly observed late increase in regenerative proliferation (at 36 hr and 48 hr) also relies on a functional  
275 apoptotic pathway, and moreover, to what extent this regenerative proliferation relies on the JNK-mediated  
276 apoptosis at the WE versus the JNK-independent NiA in the LP. To answer these questions, we blocked  
277 apoptosis throughout the pouch and this time examined proliferation in late regeneration using EdU (Figure  
278 3D-D’’). We found that the significant increase in EdU signaling at 36 hr is lost (Figure 3D’’ and F), although  
279 by 48 hr this increase is mostly restored (Figure 3D’’’ and F). Importantly, the expression of *mir(RHG)* does  
280 not influence EdU levels in the absence of damage (Figure 3 – figure supplement 1B, C and D). Together,  
281 these data confirm that a functional apoptotic pathway is necessary to induce increases in proliferation late  
282 in regeneration following necrosis. To understand the relative contribution of WE apoptosis or the NiA in the  
283 LP, we designed experiments to block apoptosis in each disc area alone (*LP>mir(RHG)*, Figure 3I, and  
284 *WE>mir(RHG)*, Figure 3J, see Materials and Methods for genotypes) relative to the whole pouch knock  
285 down (Figure 3G vs H). Strikingly, the high levels of EdU normally present at 36 hr are strongly reduced  
286 when apoptosis is blocked in either population (Figure 3K-O), suggesting that dying cells at the WE and the  
287 NiA in the LP both contribute to regenerative proliferation following necrosis. These data agree with our  
288 previous findings that the overall ability to regenerate adult wings is dependent on both populations (Klemm  
289 *et al.* 2021).

290

### 291 **NiA does not promote proliferation through Apoptosis-induced Proliferation (AiP).**

292 The question remains as to how NiA promotes regenerative proliferation. In *Drosophila*, cells undergoing  
293 apoptosis secrete factors such as Wg and Dpp to induce the proliferation of neighboring cells as part of a  
294 JNK-dependent Apoptosis-induced Proliferation (AiP) (Fogarty and Bergmann 2017). Although NiA occurs  
295 independent of JNK, to determine whether NiA-induced proliferation relies on any of the same signaling  
296 factors as AiP, we examined the damage-specific expression of these various secreted factors. To ensure  
297 we could visualize such signals, we used *lacZ*-based reporters and generated undead cells by expressing  
298 the baculoviral P35 (*UAS-P35*) in the whole pouch. This protein inhibits activity of the effector caspases  
299 Drice and Dcp-1 to block cell death (Hay *et al.* 1994), thus allowing signals produced by these cells to be  
300 readily detected. Following ablation with *DC<sup>GluR1</sup>*, ectopic *wg* and *dpp* expression (*wg-lacZ* and *dpp-lacZ*) is  
301 observed at the WE (Figure 4C and C’ vs A-B’, and Figure 4F and F’ vs D-E’, arrowheads in C’ and F’)

302 coinciding with JNK activity in this region (Klemm *et al.* 2021). However, *lacZ* is not observed in the LP  
303 where NiA occurs (Figure 4C' and F', open arrowheads), indicating that these cells do not activate these  
304 mitogens. Similarly, we did not see expression of the EGF ligand *spitz* (*spi-lacZ*) in *DC<sup>GluR1</sup>* ablated discs  
305 (Figure 4 – figure supplement 1A and B), which is observed during AiP in the eye (Fan *et al.* 2014). These  
306 results suggest that NiA does not promote proliferation through the same signaling factors as those seen  
307 during AiP.

308 We also tested whether other elements required for AiP are involved in NiA-induced proliferation. In addition  
309 to mitogen production, AiP also involves the production of extracellular reactive oxygen species (ROS)  
310 through a non-apoptotic function of Dronc that activates Duox. (Fogarty *et al.* 2016, Fogarty and Bergmann  
311 2017, Amcheslavsky *et al.* 2018, Diwanji and Bergmann 2018). We first examined the extent of ROS  
312 production using dihydroethidium (DHE). This assay showed high levels of ROS localized to the WE but not  
313 in the LP (Figure 4G, arrowhead), suggesting that NiA does not produce ROS during regeneration.  
314 Consistent with this finding, the removal of ROS through pouch-wide expression of either the ROS chelators  
315 *Catalase* and *Superoxide dismutase 1* (*UAS-Cat*; *UAS-Sod1*) or knockdown of *Duox* (*UAS-Duox<sup>RNAi</sup>*) has no  
316 observable effect on the appearance of NiA (Figure 4H and I), although apoptosis at the WE is strongly  
317 suppressed in both experiments (Figure 4H and I, open arrowhead). It has also been shown that the Duox  
318 maturation factor *moladietz* (*mol*) is upregulated following injury to sustain the production of ROS (Khan *et al.*  
319 2017, Pinal *et al.* 2018). However, while a minor increase in the expression of a *mol* reporter (*mol-lacZ*)  
320 occurs at the WE (Figure 4 – figure supplement 1C and D, arrowhead in D), no change in *lacZ* is observed  
321 in response to necrosis in the LP. Finally, to functionally test whether AiP is required for the proliferation  
322 associated with NiA, we examined EdU levels across the disc at 36 hr when P35 is expressed. Normally,  
323 when undead cells are created via P35, ectopic mitogen production results in increased proliferation and  
324 tumorous overgrowth. However, when P35 is expressed solely in the LP we saw no change in EdU labeling  
325 versus controls (Figure 4J, L and M), suggesting NiA do not form undead cells. When expressed in the  
326 whole pouch, P35 has a small but non-significant effect on EdU (Figure 4J, K and M), consistent with  
327 undead cells now being generated at the WE. Together, these data indicate that cells at the WE undergo  
328 AiP to contribute to regenerative proliferation, while NiA promote proliferation through a different  
329 mechanism.

330

### 331 **A subset of cells undergoing NiA are both caspase-positive and have markers of DNA repair** 332 **and proliferation.**

333 Robust populations of NiA appear in the wing pouch at around 18 hr of regeneration, (Figure 3 and (Klemm  
334 *et al.* 2021), while a strong increase in EdU labeling that encompasses much of the damaged pouch is  
335 detected later in regeneration at 36 hr and 48 hr (Figure 3B'', E and F). Since the loss of NiA abolishes this

336 change in proliferation (Figure 3M and O), we sought to understand how NiA might be influencing  
337 proliferation at these later time points. To do so, we used a highly sensitive sensor for the activity of the  
338 effector caspases Dcp-1 and Drice, *Green Caspase-3 Activity Indicator (UAS-GC3Ai*, (Schott *et al.* 2017) to  
339 label NiA throughout regeneration (Figure 5A-E). With this reporter we found that, unlike normal apoptotic  
340 cells that are rapidly cleared from the wing disc (Figure 5J'), NiA persist at 36 hr when proliferation  
341 strengthens (Figure 5C), as well as at 48 hr (Figure 5D), and even up to 64 hr (wandering stage (Figure 5E),  
342 when regeneration is complete and pouch tissue is restored (Figure 5E, arrowhead). These persistent  
343 GC3Ai-positive cells are also frequently associated with cells actively undergoing mitosis by 36 hr, indicated  
344 by PH3 labelling (Figure 5F). Since the position of NiA cells change over time from 18 hr when they first  
345 appear to 36 hr when the uptick in proliferation occurs, to confirm that these GC3Ai-positive cells originally  
346 derive from NiA in the LP rather than the WE, we restricted GC3Ai expression to this part of the pouch  
347 (*LP>GC3Ai*, Figure 5G and H). The GC3Ai construct is tagged with an HA epitope that can be used to show  
348 its expression even in the absence of activation by caspases (Figure 5 – figure supplement 1A and B), which  
349 we used to confirm that its expression is limited to the LP (Figure 5G and H, Figure 5 – figure supplement  
350 1C). With this experimental setup, we found that GC3Ai-positive cells are still present throughout the pouch  
351 at 36 hr (Figure 5G open arrowhead versus 5H arrowhead), confirming that the source of persistent  
352 caspase-positive cells is indeed NiA rather than the WE.

353 As NiA cells appear to be maintained in the disc for an extended period, we wondered how their behavior  
354 and morphology compared to that of normal apoptotic cells. When apoptosis is induced in wing discs using  
355 *DC<sup>hepCA</sup>*, GC3Ai labeling shows apoptotic cells present in the pouch at 18 hr (Figure 5I) throughout the disc  
356 proper (Figure 5I'). At 36 hr these cells appear pyknotic and are basally extruded by 64 hr (Figure 5J-J'). By  
357 comparison, upon ablation with *DC<sup>GluR1</sup>*, caspase-positive cells are seen to occupy different regions of the  
358 disc at 18 hr, with WE apoptotic cells closer towards the basal surface and NiA derived from the LP still  
359 within the disc proper (Figure 5K and K'). By 36 hr, the NiA form two distinct populations, some that are  
360 rounded up and appear closer to the basal surface, similar to the WE cells (Figure 5L and L' red arrowhead  
361 in L'), and others that continue to exhibit a columnar appearance and contact both the apical and basal  
362 surfaces of the disc (Figure 5L and L', yellow arrowheads in L'). The appearance and position of these cells  
363 suggest that a proportion of NiA cells may fail to complete apoptosis but instead persist into late stages of  
364 regeneration, despite the presence of detectable caspase activity. This is supported by the observation that  
365 only a minority of GC3Ai-positive cells have blebbing and pyknotic nuclei (Figure 5F', red arrowhead), while  
366 the majority appear to have a consistent and undisturbed cytoplasmic fluorescent label (Figure 5F', yellow  
367 arrowhead). To test our hypothesis that these cells are not undergoing apoptosis, we performed a TUNEL  
368 assay to fluorescently label cells with double stranded DNA breaks in GC3Ai-expressing discs. We found  
369 that most GC3Ai-labeled cells are co-labeled by TUNEL in early (18 hr) and late (36 hr) stages of  
370 regeneration (Figure 5 – figure supplement 1D and E). However, while TUNEL is associated with apoptosis,

371 by itself it does not confirm that cells are dying (Grasl-Kraupp *et al.* 1995). Therefore, we also examined  
372 levels of  $\gamma$ H2Av, a histone variant associated with DNA repair and inhibition of apoptosis following damaging  
373 stimuli such as irradiation (Madigan *et al.* 2002). Interestingly, we found that GC3Ai-positive cells initially  
374 have high levels of  $\gamma$ H2Av at 18 hr of regeneration, including those at the WE and the NiA (Figure 5 – figure  
375 supplement 1F, arrowheads), which is later lost from the NiA at 36 hr (Figure 5 – figure supplement 1G,  
376 open arrowheads). This indicates that NiA are undergoing active DNA repair rather than apoptosis. Taken  
377 together, these data suggest that a majority of NiA may upregulate caspase activity, but rather than  
378 undergoing apoptosis, they repair cellular damage and persist in the tissue into late stages of regeneration  
379 where they promote proliferation. As such, we are distinguishing this population of persistent and potentially  
380 non-apoptotic NiA by referring to them as Necrosis-induced Caspase Positive (NiCP) cells.

381

### 382 **NiCP cells have initiator caspase activity but sublethal effector caspase activity.**

383 The question remains as to why some cells (NiA) undergo apoptosis and are removed from the tissue in  
384 response to necrosis, while others (NiCP) persist despite caspase activity. The ability for cells to survive  
385 caspase activity is not surprising, as many non-apoptotic roles for caspases have been documented (Su  
386 2020), including promoting proliferation. As mentioned, the initiator caspase Dronc functions in a non-  
387 apoptotic role to activate Duox and thus promote proliferation during AiP in damaged wing discs (Fogarty *et al.*  
388 2016). Therefore, we wondered whether the difference between NiA and NiCP might arise from the level  
389 or activity of caspases within these cells. The GC3Ai reporter indicates activity of Dcp-1 and Drice (Schott *et al.*  
390 2017) while the anti-cleaved-Dcp-1 antibody is thought to also detect Drice (Li *et al.* 2019). Thus, these  
391 tools exclusively detect effector caspases. To gain a better understanding of caspase activity in NiCP we  
392 used two additional methods: the Drice-Based Sensor (*DBS-GFP*), which provides a readout for activity of  
393 the initiator caspase Dronc (Baena-Lopez *et al.* 2018), and CasExpress, a *GAL4*-based tool that provides a  
394 readout for the activity of both effector caspases Drice and Dcp-1 (Ding *et al.* 2016), but unlike the other  
395 effector caspase monitoring tools we have used, its sensitivity can be modulated via *GAL80<sup>ts</sup>* (Colon Plaza  
396 and Su 2024). Our results show a strong overlap of *DBS-GFP* with anti-Dcp-1 in the LP of *DC<sup>GluR1</sup>* ablated  
397 discs (Figure 6A and A'), indicating that these cells have robust Dronc activity, as do the cells at the WE  
398 (Figure 6A and A'). However, when we used CasExpress to examine effector caspase activity with a  
399 protocol that eliminates background developmental caspase activity (Colon Plaza and Su 2024), we noted  
400 that only cells at the WE were labelled (Figure 6B, B' and B'', arrowhead in B''), most of which had pyknotic  
401 nuclei showing they are actively undergoing apoptosis, while few cells in the LP were labelled (Figure 6B'',  
402 open arrowhead). We hypothesized that the level of effector caspase activity might be high enough to be  
403 detected by GC3Ai and the Dcp-1 antibody, but not by CasExpress. To further test this idea, we attempted  
404 to detect NiCP with CasExpress by combining it with GTRACE (Evans *et al.* 2009), which should lineage  
405 trace cells that have effector caspase activity, permanently labeling them with GFP at the start of ablation.

406 Again, we found that only cells of the WE are labelled during regeneration (Figure 6B''', arrowhead), with  
407 minimal labelling of cells in the LP (Figure 6B''', open arrowhead), even after 36 hr of regeneration when the  
408 NiCP-induced uptick in proliferation occurs (Figure 6 – figure supplement 1A). By comparison, performing  
409 these same experiments using  $DC^{hepCA}$  to induce extensive apoptotic cell death leads to a significant  
410 proportion of Dcp-1-positive cells being labelled by CasExpress under both normal and lineage tracing  
411 conditions despite their ongoing elimination (Figure 6C, arrowheads), suggesting that in the context of  
412 necrosis there is not enough effector caspase activity to label NiCP using these methods. Indeed, if the  
413 CasExpress experiment is performed in the absence of the  $GAL80^{fs}$  that suppresses the background  
414 developmental caspase signal, the NiCP cells now become labeled by GFP (Figure 6D), indicating that  
415 effector caspases are indeed present in these cells, but at potentially low enough levels to avoid death.  
416 Evidence for the existence of a cellular execution threshold of caspase activity in cells of the wing disc,  
417 which must be reached to induce apoptosis, has previously been documented (Florentin and Arama 2012).  
418 This is further supported by the observation that the GFP label becomes more apparent later in regeneration  
419 (Figure 6E), confirming that cells with effector caspase activity persist rather than die. Thus, it appears that  
420 in response to necrosis, the cells of the LP activate the initiator caspase Dronc and the effector caspase(s)  
421 Drice/Dcp-1 (to an extent) but fail to undergo programmed cell death. Instead, these cells persist in the disc  
422 late into regeneration where they stimulate regenerative proliferation.

#### 423 424 **Dronc in NiCP cells promote proliferation independent of AiP.**

425 While NiCP cells have both initiator (Dronc) and effector caspase (Drice/Dcp-1) activity, it appears that the  
426 level or function of effector caspases is insufficient to cause apoptosis, and is also inconsequential for  
427 promoting regeneration – indeed, blocking Drice/Dcp-1 activity with P35 does not affect the increase in  
428 regenerative proliferation observed at 36 hr (Figure 4L and M), or the overall ability to regenerate (Klemm *et al.* 2021). This is in contrast with the ability of effector caspases to drive proliferation in the eye disc (Fan  
429 and Bergmann 2008). However, blocking the apoptotic pathway upstream of Dronc using *mir(RHG)*  
430 eliminates NiA/NiCP (Figure 7A, C and K, (Klemm *et al.* 2021), blocks the increase in proliferation (Figure  
431 7B, D and L), and limits regeneration (Klemm *et al.* 2021). These observations demonstrate that proliferation  
432 induced by NiCP must depend on factors downstream of Rpr/Hid/Grim and upstream of the effector  
433 caspases Drice/Dcp-1, thus potentially pointing to a role for Dronc. To test this, we ablated discs with  
434  $DC^{GluR1}$  while reducing the activity of Dronc using a null allele ( $Dronc^{J29/+}$ , (Xu *et al.* 2005)). With this genetic  
435 background there is a significant reduction in regenerative proliferation at 36 hr (Figure 7F and L, open  
436 arrowhead in F) and regeneration is limited, shown by both adult wing scores (Figure 7M) and wing size  
437 (Figure 7 – figure supplement 1A). These data demonstrate an essential role for Dronc in NiCP to promote  
438 proliferation and subsequent regeneration of the disc following necrosis. We noted that this mutant does not  
439 strongly affect the appearance of Dcp-1 (Figure 7E and K), likely because this allele does not completely  
440

441 suppress apoptosis, and thus the Dcp-1 label, unless homozygous (Xu *et al.* 2005), which is precluded by  
442 the genetics of this experiment. As an alternative, we interfered with Dronc function by expressing a  
443 dominant negative form of *Dronc* that contains only the caspase recruitment (CARD) pro-domain, here  
444 referred to as *Dronc<sup>DN</sup>*, which blocks activation of Dcp-1/Drice and apoptosis (Meier *et al.* 2000). *Dronc<sup>DN</sup>*  
445 reduces NiCP number, but to a lesser degree than *mi(RHG)* (Figure 7G and K) and does not affect  
446 proliferation (Figure 7H and L), suggesting that the CARD domain is dispensable for NiCP-induced  
447 proliferation.

448 Finally, we wondered how this might relate to the previously documented role of Dronc in promoting  
449 proliferation following apoptotic cell death during AiP (Fogarty and Bergmann 2017). AiP depends on both  
450 JNK and ROS (Fogarty *et al.* 2016), which we have shown are only present at the WE and are not  
451 associated with NiA/NiCP (Figure 4G, H and I). Thus, it is possible that Dronc's function in response to  
452 necrosis occurs via a distinct mechanism. Importantly, the activity of Dronc in both apoptosis and in AiP is  
453 influenced by Dronc's upstream regulator, DIAP1 (Meier *et al.* 2000). DIAP1 modifies Dronc's CARD domain  
454 to block both apoptosis (Kamber Kaya *et al.* 2017), and AiP (Fan and Bergmann 2008, Fogarty and  
455 Bergmann 2017). Thus, we expressed *DIAP1 (UAS-DIAP1)* following ablation with *DC<sup>GluR1</sup>* and found that it  
456 strongly suppresses the number of Dcp-1-positive cells at the WE and the NiA/NiCP in the LP (Figure 7I and  
457 K, open arrowheads in I), but strikingly has no effect on regenerative proliferation at 36 hr (Figure 7J and L).  
458 These results demonstrate a key role for the initiator caspase Dronc in promoting regenerative proliferation  
459 following necrosis, which is not affected by DIAP1, and therefore is likely separate from its role in apoptosis  
460 and the AiP mechanism.

461 Taken together, our data suggest a model in which necrosis leads to the establishment of distinct cell  
462 populations important for regeneration (Figure 7N). After injury, cells at the immediate WE undergo JNK-  
463 mediated apoptosis and contribute to proliferation via the established AiP mechanism (Figure 7N). while  
464 cells at a distance from the injury in the LP activate Dronc via an unknown DAMP-like signal(s) that occurs  
465 independent of JNK. Some of these cells go on to activate effector caspases at levels high enough to result  
466 in apoptosis (NiA, Figure 7N), while others activate these caspases at a low enough level to be detectable  
467 but insufficient to induce death (NiCP, Figure 7N). Instead, these cells persist in the tissue late into the repair  
468 process, where they promote proliferation via a novel non-apoptotic and AiP-independent function of the  
469 initiator caspase Dronc.

## 470 Discussion

471 An important and often overlooked factor when studying regeneration is the type of injury, and consequently  
472 the type of cell death it causes, which significantly impacts the repair processes. The existence of conserved  
473 signaling events that promote recovery has been well established in the context of apoptosis (Fogarty and  
474 Bergmann 2017, Perez-Garijo 2018), while the importance of such events in necrosis are less understood.  
475 Here, we have investigated the genetic events that occur in the aftermath of necrosis and how they influence  
476 the ability of a tissue to recover and regenerate. We previously showed that wing discs can regenerate  
477 effectively in the face of necrotic cell death (Klemm *et al.* 2021), triggering local JNK-dependent AiP at the  
478 WE, which is likely in response to tissue disruption (La Marca and Richardson 2020), while also inducing  
479 caspase activity in cells at a distance from the wound. This induction is independent of JNK signaling and,  
480 alongside having effector caspase activity, these cells can be marked by TUNEL and be blocked by  
481 inhibiting the apoptotic pathway (Klemm *et al.* 2021). As such, we determined that these cells are  
482 undergoing PCD and named this phenomenon Necrosis-induced Apoptosis (NiA). We also showed that both  
483 NiA and AiP at the wound contribute to regeneration. Our current work further characterizes the NiA  
484 phenomenon, and we have now shown that cells undergoing NiA in fact comprise two populations with  
485 separate behaviors. Upon necrosis, cells of the LP appear to activate effector caspases, indicated by  
486 cleaved Dcp-1 antibody staining and activation of the transgenic reporter GC3Ai. While a proportion of these  
487 cells develop apoptotic morphology, round up and are cleared over time as part of NiA, a large number of  
488 cells appear able to persist despite the presence of caspases, where they promote regenerative proliferation  
489 dependent on the initiator caspase Dronc (Figure 7N). To reflect these new findings, we have called these  
490 Necrosis-induced Caspase Positive (NiCP) cells. As these events occur in the absence of JNK, and exhibit  
491 none of the established hallmarks of AiP, including the presence and requirement for ROS, the ability to be  
492 blocked by DIAP1, or the production of mitogens such as Wg and Dpp, our results have identified an new  
493 function of Dronc in promoting regeneration in response to necrotic cell death.

### 494 **The signal from necrotic cells that leads to NiA/NiCP is unknown.**

495 Although we have shown that necrosis leads to NiCP cells and NiA at a distance from the site of injury, the  
496 signal that leads to these events is still unknown. Cells undergoing necrosis release DAMPs, a category of  
497 molecules that includes both common cellular contents as well as specific proteins, both of which can  
498 produce downstream responses like inflammation and the activation of effectors that promote a healing  
499 response (Gordon *et al.* 2018). DAMPs of both categories have been demonstrated in *Drosophila*; in  
500 apoptosis-deficient larvae, circulating DAMPs in the hemolymph can constitutively activate immune signaling  
501 in the fat body (Nishida *et al.* 2024), while specific factors such as  $\alpha$ -actinin (Gordon *et al.* 2018), and  
502 HMGB1 (Nishida *et al.* 2024) are known to possess DAMP activity. Recent work describing an *in vivo* sensor  
503 for HMGB1 demonstrates the release of this DAMP from wing disc cells in response to a necrotic stimulus

504 similar to that used here (Nishida *et al.* 2024), making this an important candidate to test for a potential role  
505 in producing NiCP. However, it is equally possible that the causative DAMP(s) is one or more of the  
506 common fundamental cellular components released upon cell lysis, which would be more challenging to test.  
507 Considering the potential diversity and variable nature of DAMPs, it may be more feasible to instead identify  
508 the downstream PRRs that are required to interpret this unknown signal. Several groups of genes can act  
509 as PRRs, most notably the Toll-like receptor (TLR) family, various members of which can respond to DAMPs  
510 (Ming *et al.* 2014, Gong *et al.* 2020). Nine TLR genes have been identified in *Drosophila*, which have  
511 assorted roles in development and innate immunity (Anthony *et al.* 2018), and have been implicated in  
512 DAMP sensing (Ming *et al.* 2014). Thus, it would be valuable to test the requirement for TLRs, alongside  
513 other suspected PRRs such as scavenger receptors (Cao 2016, Roh and Sohn 2018, Gong *et al.* 2020) for  
514 their requirement to induce NiCP.

515 An additional approach to elucidating how these cells are generated is by leveraging our finding that both  
516 JAK/STAT and WNT signaling seem to block NiCP/NiA in the disc. JAK/STAT signaling promotes survival of  
517 cells in response to stress by repressing JNK signaling, thus minimizing JNK-mediated apoptosis (La  
518 Fortezza *et al.* 2016). Although NiCP appear to avoid damage-induced JAK/STAT upregulation in the pouch,  
519 it is unlikely that this mechanism is responsible, since NiCP cells occur independent of JNK activity (Klemm  
520 *et al.* 2021). However, within the hinge, which is completely devoid of NiCP, JAK/STAT protects cells from  
521 apoptosis potentially by upregulating *DIAP1* (Verghese and Su 2016) and *zfh2* (Verghese and Su 2018),  
522 while Wg represses the transcription of *rpr*, (Verghese and Su 2016). Both signaling pathways are required  
523 autonomously in hinge cells for their ability to replace and regenerate ablated pouch tissue (Verghese and  
524 Su 2016, Ledru *et al.* 2022). Our results show that DIAP1 can prevent Dcp-1 activation in NiCP in the pouch,  
525 but not the corresponding proliferation that they produce, suggesting one reason that NiCP is not seen in the  
526 hinge is possibly due to the high DIAP1 threshold, which blocks Dronc's ability to activate effector caspases  
527 in this region. This may be in addition to a role for the JAK/STAT target *Zfh2*, which negatively regulates  
528 NiCP in the pouch. Thus, it remains to be seen whether lowering DIAP1 levels in the hinge, or manipulating  
529 Wg to allow *rpr* expression alongside changes in JAK/STAT and/or *zfh2*, might alter the appearance of NiCP  
530 in this region. Finally, the observation that both NiCP cells and their associated proliferative effects appear to  
531 occur independent of JNK signaling, which is normally central in models of stress and damage (Pinal *et al.*  
532 2019), could help to narrow the identity of upstream signaling factors that leads to NiCP following necrosis.  
533 Together, these approaches could provide essential information as to the underlying genetic and cellular  
534 events that connect the lysis of cells during necrosis to the formation of NiCP cells required for regeneration.

### 535 **The persistence of NiCP cells versus their elimination via NiA.**

536 Our work shows that cells in the LP can either persist as NiCP and contribute to regenerative proliferation, or  
537 progress to apoptosis as part of NiA, but how this decision is made is unknown. During apoptosis in the wing  
538 disc, a threshold level of effector caspases must be reached for the cell to complete PCD (Florentin and

539 Arama 2012). Thus, we hypothesize that DAMP signals from necrotic cells may result in inconstant levels of  
540 effector caspase activity in cells of the LP – some with high caspases that advance to apoptosis (NiA),  
541 recognized by the changes in morphology and position in the disc characteristic of PCD, and others (NiCP  
542 cells) that have low enough caspase activity levels to survive, but this activity can still be detected by  
543 sensitized reagents. This is supported by our observations made using effector caspase-based lineage  
544 tracing using CasExpress (Ding *et al.* 2016), in which caspases can only be detected in NiCP cells by  
545 lowering the detection threshold. Alternatively, since CasExpress is a membrane-based reporter (Ding *et al.*  
546 2016), it is also possible that effector caspases within NiCP cells have a different subcellular localization that  
547 reflects a non-apoptotic function, thus preventing reporter activation, rather than a difference in expression  
548 level or activity. The idea that caspases have different functions, both apoptotic and non-apoptotic, based on  
549 localization is well established, such as the targeting of specific cleavage substrates in distinct subcellular  
550 compartments (Brown-Suedel and Bouchier-Hayes 2020), or the trafficking of Dronc to the membrane to  
551 promote ROS (Amcheslavsky *et al.* 2018). Whatever the mechanism is that distinguishes between  
552 elimination via NiA or persistence as NiCP, the proportion of LP cells that participate in each remains difficult  
553 to assay due to the dynamic nature of cell death (Nano and Montell 2024) and overall variability of the  
554 NiCP/NiA phenotype. Anecdotal evidence from our experiments examining GC3Ai-labelled cells over time  
555 suggests that most cells in fact do not undergo apoptosis and are therefore NiCP. However, the use of other  
556 tools with potentially different sensitivities to effector caspases, such as Apoliner (Bardet *et al.* 2008), or  
557 CD8-PARP-Venus (Florentin and Arama 2012), may shed further light on this issue. Nevertheless, it  
558 remains to be seen how a cell becomes NiCP or undergoes NiA and dies, and whether distinct levels of  
559 caspases (initiator or effector), their localization, or a different attribute is responsible.

560

### 561 **How does NiCP contribute to regeneration?**

562 One of the most important questions that must be addressed is how the phenomena we have identified lead  
563 to regeneration following necrosis. Our experiments suggest that different caspase-positive populations of  
564 cells may contribute to regenerative proliferation: Firstly, the smaller number of apoptotic cells at the WE that  
565 likely contribute by the established process of JNK-dependent AiP (Fogarty and Bergmann 2017). Secondly,  
566 the caspase-surviving NiCP cells in the LP that contribute via an unknown process requiring the initiator  
567 caspase Dronc. Crucially, this non-apoptotic function of Dronc cannot be inhibited by the expression of  
568 DIAP1, which has previously been shown able to block both the apoptotic and non-apoptotic AiP functions of  
569 Dronc (Meier *et al.* 2000). Thus, our results suggest that Dronc acts in a different mechanism to induce  
570 growth in response to necrosis. The current understanding of how Dronc functions at the molecular level  
571 may provide valuable clues as to how. DIAP1 suppresses Dronc through its E3 ubiquitin ligase activity,  
572 which mono-ubiquitylates the CARD domain of Dronc to suppress both apoptotic and non-apoptotic  
573 functions related to AiP (Meier *et al.* 2000). Here, we find that the ectopic expression of *DIAP1* or just the

574 CARD-containing pro-domain of Dronc (*Dronc<sup>DN</sup>*) cannot block regenerative proliferation while, by contrast,  
575 heterozygosity for the *Dronc<sup>J29</sup>* null allele that can inhibit AiP (Kamber Kaya *et al.* 2017), is sufficient to block  
576 NiCP-mediated proliferation. Thus, regulation of Dronc activity in the context of necrosis may not rely on the  
577 modification of its CARD domain. Dronc's documented functions can also require its catalytic domain;  
578 mutations in this domain block the activation of Drice, and AiP-induced overgrowth (Fan *et al.* 2014). Thus, it  
579 will be important to assay whether the catalytic domain of Dronc is necessary to induce regenerative  
580 proliferation via NiCP. Similarly, although the CARD and catalytic domains are important points of regulation  
581 for Dronc activity, it has also been shown that damage-specific context cues are also vital. For example, the  
582 ectopic expression of *Dronc<sup>K78R</sup>*, a mutant that cannot be repressed by DIAP1, might be expected to induce  
583 significant apoptotic cell death. However, this is not the case unless its structural binding partner, the APAF1  
584 ortholog encoded by *Dark*, is expressed alongside (Shapiro *et al.* 2008), demonstrating the importance of  
585 stoichiometry between Dronc and Dark for the apoptotic function of Dronc. As such, further investigation into  
586 Dronc's functional domains and context-dependent interactions with its binding partners, including DIAP1  
587 and Dark, will likely be necessary to understand how Dronc is involved in promoting regenerative  
588 proliferation in response to necrotic injury.

589

#### 590 **NiCP as a general mechanism to promote regeneration**

591 Although initially characterized for their central role in apoptosis, many non-apoptotic functions of caspases  
592 have since been discovered, showing them to be dynamic regulators of diverse processes including cell fate  
593 specification, cellular remodeling, tissue growth, development, metabolism and others (Shinoda *et al.* 2019,  
594 Wang and Baker 2019, Su 2020). Studies of caspase signaling during regeneration have revealed essential  
595 non-apoptotic activities, such as initiator and effector-dependent models of AiP that contribute to repair  
596 (Ryoo and Bergmann 2012, Fogarty and Bergmann 2017). The contrasts in caspase functions that we have  
597 observed between apoptotic and necrotic damage, despite ultimately resulting in comparable levels of  
598 regeneration (Klemm *et al.* 2021), underscores the nuance that exists in damage signaling between different  
599 injury contexts. It is clear that caspase activity in response to injury as a mechanism to promote regeneration  
600 is a highly conserved process that occurs in many organisms, regardless of tissue identify or type of damage  
601 incurred (Bergmann and Steller 2010, Vriza *et al.* 2014, Fuchs and Steller 2015, Perez-Garijo and Steller  
602 2015, Fogarty and Bergmann 2017, Perez-Garijo 2018). Our findings reinforce the position that we still have  
603 much to learn about the role of caspases in tissue repair, and that the type of injury, and thus the nature of  
604 cell death involved, is a vital consideration when developing effective wound-healing strategies.

## 605 **Materials and Methods**

### 606 **Drosophila stocks**

607 Flies were cultured in conventional dextrose fly media at 25°C with 12h light–dark cycles. The recipe for  
608 dextrose media contains 9.3 g agar, 32 g yeast, 61 g cornmeal, 129 g dextrose, and 14 g tegosept in 1 L  
609 distilled water. Genotypes for each figure panel are listed in the Supplementary Genotypes file. Fly lines  
610 used as ablation stocks are as follows: hs-FLP; hs-p65; salm-LexADBD, DVE>>GAL4 (DC<sup>NA</sup>), hs-FLP; hs-  
611 p65; salm-LexADBD/ TM6C, sb (DC<sup>NA</sup> no GAL4), hs-FLP; lexAop-GluR1<sup>LC</sup>, hs-p65/ CyO; salm-LexADBD,  
612 DVE>>GAL4/ TM6B, Tb (DC<sup>GluR1</sup>), hs-FLP; lexAop-GluR1<sup>LC</sup>, hs-p65/CyO; salm-LexADBD/TM6C, sb  
613 (DC<sup>GluR1</sup> no GAL4), hs-FLP; lexAop-GluR1<sup>LC</sup>/ CyO; salm-LexADBD, hh-GAL4/ TM6B, Tb (DC<sup>GluR1</sup> hh-GAL4),  
614 hs-FLP; lexAop-hepCA, hs-p65/CyO; salm-DBD, DVE>>GAL4/ TM6B, Tb (DC<sup>hepCA</sup>), UAS-GluR1;  
615 tubGAL80<sup>ts</sup>, and tubGAL80<sup>ts</sup>. The stock DR<sup>WNT</sup>-GAL80 was used to limit *UAS*- transgenes to the lateral  
616 pouch (LP) where NiA occur (Klemm *et al.* 2021), while *R85E08-GAL4* was used to drive *UAS*- expression  
617 at the wound edge (WE). The following stocks were obtained from Bloomington Drosophila Stock Center:  
618 UAS-*y*<sup>RNAi</sup> (BL#64527), UAS-p35 (BL#5073), UAS-hepCA (BL#58981), UAS-GC3Ai (II, BL#84346), UAS-  
619 GC3Ai (III, BL#84343), rn-GAL4 (BL#7405), hh-GAL4 (BL#600186), ptc-GAL4 (BL#2017), pnr-GAL4 (BL#),  
620 (BL#25758), nub-GAL4 (BL#25754), R73G07-GAL4 (BL#39829), UAS-Zfh2RNAi (BL#50643), UAS-wg<sup>RNAi</sup>  
621 (BL#32994), UAS-Stat92ERNAi (BL#35600), UAS-TCF<sup>DN</sup> (II, BL#4784), dpp-lacZ (BL#8412), wg-lacZ  
622 (BL#50763), spi-lacZ (BL#10462), UAS-p35 (II, BL#5072), UAS-p35 (III, BL#5073), AP-1-GFP (Chatterjee  
623 and Bohmann 2012), act>>GAL4, UAS-RFP (BL#30558), DBS-GFP (III, BL#83130), DBS-QF (BL#83131),  
624 QUAS-FLP, act>>lacZ (BL#83133), CasExpress (BL#65419), G-trace (III, BL#28281), tubGAL80<sup>ts</sup> (II,  
625 BL#7019), tubGAL80<sup>ts</sup> (III, BL#7017), 10xSTAT-GFP (BL#), UAS-dome<sup>RNAi</sup> (BL#32860), UAS-hop48A (BL#),  
626 PCNA-GFP (BL#25749), UAS-Cat (BL#24621), UAS-Sod1 (BL#24754), UAS-Duox<sup>RNAi</sup> (BL#32903), mol-  
627 lacZ (BL#12173), rpr-lacZ (BL#98451), UAS-rpr<sup>RNAi</sup> (BL#51849), UAS-dronc<sup>RNAi</sup> (BL#32963), UAS-Dronc<sup>DN</sup>  
628 (BL#58992), UAS-Strica<sup>RNAi</sup>, UAS-DIAP1 (BL#6657), UAS-Dcp-1<sup>RNAi</sup> (BL#38315), UAS-Drice<sup>RNAi</sup>  
629 (BL#32403), and dronc<sup>I29</sup>/TM3, Sb (BL#98453). UAS-mir(RHG) was gifted from the Hariharan lab at UC  
630 Berkeley. vgQE-lacZ was gifted from Tin Tin Su. UAS-GluR1<sup>LC</sup> (Liu *et al.* 2013) was gifted from the Xie lab  
631 at Stowers Institute.

632

### 633 **Ablation experiments**

634 **DUAL Control ablation with DVE>>GAL4.** DUAL Control experiments were performed essentially as  
635 described in Harris *et al.* (2020). Briefly, experimental crosses were cultured at 25°C and density controlled  
636 at 50 larvae per vial. Larvae were heat shocked on 3.5 of development (84 hr after egg deposition (AED)) by  
637 placing vials in a 37°C water bath for 45 min, followed by a return to 25°C. Larvae were allowed to recover  
638 for 18 hr before being dissected, fixed and immunolabeled, unless otherwise indicated. UAS-*y*<sup>RNAi</sup> and UAS-

639 GFP were used as control lines for RNAi-based experiments.  $w^{1118}$  was used as a control for *Dronc*<sup>l29</sup>  
640 experiments. *DVE>>GAL4* drives expression in the wing pouch, allowing for the regenerating wound edge  
641 cells and NiA cells to be targeted for interrogation (Klemm *et al.* 2021). The *DR<sup>WNT</sup>-GAL80* transgene  
642 (Klemm *et al.* 2021) was included as necessary to restrict *UAS*- expression to the LP where NiA/NiCP  
643 occurs.

644

645 **DUAL Control ablation without *DVE>>GAL4*.** To restrict *UAS*- expression to WE apoptotic cells, a version  
646 of DUAL Control lacking the *DVE>>GAL4* (*DC<sup>GluR1</sup> no GAL4*) was crossed to the *R85E08-GAL4* driver.

647 *DC<sup>GluR1</sup> no GAL4* experiments were performed along the same parameters as *DC<sup>GluR1</sup>* experiments.

648

649 **DUAL Control ablation with *hh-GAL4*.** DUAL Control flies bearing *hh-GAL4* (*DC<sup>GluR1</sup> hh<sup>ts</sup>*) were cultured at  
650 18°C and density controlled at 50 larvae per vial. *tubGAL80<sup>ts</sup>* was included to conditionally express *UAS*-  
651 based constructs after ablation. Larvae were heat-shocked on day 7 of development (168 hr AED) for 45  
652 min at 37°C, followed by incubation at 30°C to inactivate *tubGAL80<sup>ts</sup>* and permit *UAS*-based expression.  
653 Larvae were allowed to recover for 18 hr before being dissected, fixed, and immunolabeled.

654

655 ***GAL4/UAS* ablation.** *GAL4/UAS*-based ablation experiments were performed essentially as described in  
656 Smith-Bolton *et al.* (2009). Briefly, larvae bearing *UAS-GluR1*; *tubGAL80<sup>ts</sup>* were cultured at 18°C and density  
657 controlled at 50 larvae per vial. Larvae upshifted on day 7 of development (168 hr AED) for 20 hr at 30°C  
658 and were either immediately dissected (denoted as 0 hr) or were allowed to recover for 24 hr before being  
659 dissected, fixed, and imaged. *tubGAL80<sup>ts</sup>* flies were used as a non-ablating control.

660

661 ***FLP/FRT* ablation experiments.** To generate clonal patches of *UAS-GluR1*; *UAS-RFP*-expressing cells,  
662 flies of the genotype *hs-FLP*; *AP-1-GFP*; *act>>GAL4*, *UAS-RFP*/ *T(2:3)SM6A*, *TM6B*, *Tb* were crossed to  
663 flies bearing *UAS-GluR1*; *tubGAL80<sup>ts</sup>*. Larvae were cultured at 18°C and heat shocked in a 37°C water bath  
664 for 10 min at 42 hr AEL, returned to 18°C, and upshifted to 30°C for 18 hr at 168 h AEL, followed by  
665 dissection and immunostaining. *tubGAL80<sup>ts</sup>* flies were used as a non-ablating control.

666

667 **Regeneration scoring and wing measurements.**

668 Adult wings were scored and measured after genotype blinding by another researcher. Scoring was  
669 performed on anesthetized adults by binning into a regeneration scoring category (Harris *et al.* 2020, Klemm  
670 *et al.* 2021). Wing measurements were performed by removing wings, mounting in Permount solution  
671 (Fisher Scientific) and imaged using a Zeiss Discovery.V8 microscope. Wing area was measured using the  
672 Fiji software. Male and female adults were measured separately to account for sex differences in wing size

673 using a reproducible measuring protocol that excludes the variable hinge region of the wing (details of  
674 measuring protocol available on request). Statistics were performed using GraphPad Prism 10.0.

675

## 676 **Immunohistochemistry**

677 Larvae were dissected in 1 x PBS followed by a 20 min fix in 4 % paraformaldehyde in PBS (PFA). After 3  
678 washes in 0.1 % PBST (1 x PBS + 0.1 % Triton-X), larvae were washed in 0.3% PBST and then blocked in  
679 0.1 % PBST with 5 % normal goat serum (NGS) for 30 min. Primary staining was done overnight at 4°C, and  
680 secondary staining was done for 4 hr at room temperature. The following primary antibodies were obtained  
681 from the Developmental Studies Hybridoma Bank: mouse anti-Nubbin (1:25), mouse anti-Wg (1:100),  
682 mouse anti-Mmp1 C-terminus (1:100), mouse anti-Mmp1 catalytic domain (1:100), mouse anti-LacZ (1:100),  
683 mouse anti-discs large (1:50), mouse anti-yH2Av (1:100), and rat anti-DE-cadherin (1:100). Rabbit anti-Dcp-  
684 1 (1:1000), mouse anti-PH3 (1:500), and rabbit anti-HA (1:1000) were obtained from Cell Signaling  
685 Technologies. Rat anti-Zfh-2 was generously gifted by Chris Doe. Anti-rabbit 647, anti-rat 647, anti-mouse  
686 555, and anti-mouse 488 secondary antibodies were obtained from Invitrogen and used at a 1:500 dilution.  
687 DAPI (1:1000) was used as a counterstain. Images were obtained on a Zeiss Axiolmager.M2 with ApoTome  
688 and a Leica TCS SP8 LCSM (NIH SIG award 1 S10 OD023691-01) housed in the Regenerative Medicine  
689 Imaging Facility at Arizona State University. For each experiment at least 15 discs were analyzed prior to  
690 choosing a representative image. Images were processed using Affinity Photo.

691

## 692 **EdU staining, TUNEL assay, and DHE staining**

693 **EdU.** The Click-It EdU Alexa Fluor 555 Imaging Kit (Invitrogen C10338) was used to assay cell proliferation.  
694 Briefly, imaginal discs were dissected and labeled with 1 µl EdU in 1 ml PBS for 20 min, fixed in 4 % PFA for  
695 20 min and immunolabeled (as necessary), followed by a 30 min Click-It reaction that was performed as  
696 directed in the EdU manual.

697

698 **TUNEL.** The TUNEL assay was performed with the ApopTag Red In Situ Apoptosis Detection Kit (Millipore  
699 S7165). Dissected larvae were fixed in 4 % paraformaldehyde, followed by a 10 min wash in 75 ml  
700 equilibration buffer. Discs were then submerged in 55 ml working strength TdT enzyme for 3 hr at 37°C. The  
701 reaction was stopped by adding 1ml stop/wash buffer and incubating for 10min at room temperature,  
702 followed by three washes in PBS. Immunolabeling was performed by incubating the tissue preps with 65 ml  
703 of anti-digoxigenin rhodamine overnight at room temperature.

704

705 **Dihydroethidium (DHE).** DHE labeling was performed by incubating freshly dissected wing imaginal discs  
706 in Schneider's Media with 1 µl of 10 mM DHE reconstituted in 1 ml DMSO (for a working concentration of 10  
707 µM DHE) for 10 min, followed by three 5 min washes in PBS and immediately mounting and imaging.

708

## 709 **Quantification and Statistical Analysis**

710 Adult wings, mean fluorescence intensity, and cell counts were measured using Fiji. GraphPad Prism 10.0  
711 was used for statistical analysis and graphical representation. Graphs depict the mean of each treatment,  
712 while error bars represent the standard deviation. The mean fluorescence intensity of EdU labeling was  
713 quantified in Fiji by normalizing the wing pouch to the entire disc. The sample size and P values for all  
714 statistical analyses are indicated in the figure legends. Statistical significance was evaluated in Prism 10.0  
715 using a Student's T-test or a one-way ANOVA with a multiple comparisons test.

716

## 717 **Data and reagent availability**

718 Stocks are available upon request and details of stocks and reagents used in this study are available in the  
719 materials and methods. The authors affirm that all data necessary for confirming the conclusions of the  
720 article are present within the article, figures, and tables.

721

## 722 **Acknowledgements**

723 The authors would like to thank Dr. Tin Tin Su of UC Boulder, Dr. Chris Doe of the University of Oregon, and  
724 Dr. Tian Xie of the Stowers Institute for their generous gift of stocks and reagents. We thank the current  
725 members of the Harris lab for useful input and feedback. We thank the Bloomington Drosophila Stock  
726 Center and Developmental Studies Hybridoma Bank for stocks and reagents.

727

## 728 **Funding**

729 This work was supported by a grant from the Eunice Kennedy Shriver National Institute of Child Health and  
730 Human Development (NICHD) R21HD102765-01 and the National Institute of General Medical Sciences  
731 (NIGMS) R01GM147615 to Robin Harris.

732

## 733 **Author contributions**

734 Jacob Klemm, Conceptualization, Investigation, Data curation, Formal analysis, Validation, Writing – original  
735 draft, Writing – review and editing; Chloe Van Hazel, Resources; Robin Harris, Supervision,  
736 Conceptualization, Funding acquisition, Investigation, Resources, Writing – review and editing.

737

## 738 **Conflicts of interest**

739 The authors declare that there is no conflict of interest.

740

741

742

743

744

745

746

747 **References**

- 748 1. Amcheslavsky, A., et al. (2018). "Plasma Membrane Localization of Apoptotic Caspases for Non-apoptotic  
749 Functions." *Dev Cell* **45**(4): 450-464 e453.
- 750 2. Anthony, N., et al. (2018). "Toll and Toll-like receptor signalling in development." *Development* **145**(9).
- 751 3. Ashkenazi, A. and G. Salvesen (2014). "Regulated cell death: signaling and mechanisms." *Annu Rev Cell Dev*  
752 *Biol* **30**: 337-356.
- 753 4. Bach, E. A., et al. (2007). "GFP reporters detect the activation of the Drosophila JAK/STAT pathway in vivo."  
754 *Gene Expr Patterns* **7**(3): 323-331.
- 755 5. Baena-Lopez, L. A., et al. (2018). "Novel initiator caspase reporters uncover previously unknown features of  
756 caspase-activating cells." *Development* **145**(23).
- 757 6. Bardet, P. L., et al. (2008). "A fluorescent reporter of caspase activity for live imaging." *Proc Natl Acad Sci U S*  
758 *A* **105**(37): 13901-13905.
- 759 7. Beira, J. V. and R. Paro (2016). "The legacy of Drosophila imaginal discs." *Chromosoma* **125**(4): 573-592.
- 760 8. Bergmann, A. and H. Steller (2010). "Apoptosis, stem cells, and tissue regeneration." *Sci Signal* **3**(145): re8.
- 761 9. Bonne, S. L. and S. S. Kadri (2017). "Evaluation and Management of Necrotizing Soft Tissue Infections." *Infect*  
762 *Dis Clin North Am* **31**(3): 497-511.
- 763 10. Brown-Suedel, A. N. and L. Bouchier-Hayes (2020). "Caspase-2 Substrates: To Apoptosis, Cell Cycle Control,  
764 and Beyond." *Front Cell Dev Biol* **8**: 610022.
- 765 11. Cao, X. (2016). "Self-regulation and cross-regulation of pattern-recognition receptor signalling in health and  
766 disease." *Nat Rev Immunol* **16**(1): 35-50.
- 767 12. Chatterjee, N. and D. Bohmann (2012). "A versatile PhiC31 based reporter system for measuring AP-1 and  
768 Nrf2 signaling in Drosophila and in tissue culture." *PLoS One* **7**(4): e34063.
- 769 13. Chera, S., et al. (2009). "Apoptotic cells provide an unexpected source of Wnt3 signaling to drive hydra head  
770 regeneration." *Dev Cell* **17**(2): 279-289.
- 771 14. Colon Plaza, S. and T. T. Su (2024). "Ionizing radiation induces cells with past caspase activity that contribute  
772 to the adult organ in Drosophila and show reduced Loss of Heterozygosity." *Cell Death Discov* **10**(1): 6.
- 773 15. D'Arcy, M. S. (2019). "Cell death: a review of the major forms of apoptosis, necrosis and autophagy." *Cell Biol*  
774 *Int* **43**(6): 582-592.
- 775 16. Ding, A. X., et al. (2016). "CasExpress reveals widespread and diverse patterns of cell survival of caspase-3  
776 activation during development in vivo." *Elife* **5**.
- 777 17. Diwanji, N. and A. Bergmann (2018). "An unexpected friend - ROS in apoptosis-induced compensatory  
778 proliferation: Implications for regeneration and cancer." *Semin Cell Dev Biol* **80**: 74-82.
- 779 18. Evans, C. J., et al. (2009). "G-TRACE: rapid Gal4-based cell lineage analysis in Drosophila." *Nat Methods*  
780 **6**(8): 603-605.
- 781 19. Fan, Y. and A. Bergmann (2008). "Apoptosis-induced compensatory proliferation. The Cell is dead. Long live  
782 the Cell!" *Trends Cell Biol* **18**(10): 467-473.

- 783 20. Fan, Y. and A. Bergmann (2008). "Distinct mechanisms of apoptosis-induced compensatory proliferation in  
784 proliferating and differentiating tissues in the *Drosophila* eye." *Dev Cell* **14**(3): 399-410.
- 785 21. Fan, Y., et al. (2014). "Genetic models of apoptosis-induced proliferation decipher activation of JNK and  
786 identify a requirement of EGFR signaling for tissue regenerative responses in *Drosophila*." *PLoS Genet* **10**(1):  
787 e1004131.
- 788 22. Festjens, N., et al. (2006). "Necrosis, a well-orchestrated form of cell demise: signalling cascades, important  
789 mediators and concomitant immune response." *Biochim Biophys Acta* **1757**(9-10): 1371-1387.
- 790 23. Florentin, A. and E. Arama (2012). "Caspase levels and execution efficiencies determine the apoptotic  
791 potential of the cell." *J Cell Biol* **196**(4): 513-527.
- 792 24. Fogarty, C. E. and A. Bergmann (2017). "Killers creating new life: caspases drive apoptosis-induced  
793 proliferation in tissue repair and disease." *Cell Death Differ* **24**(8): 1390-1400.
- 794 25. Fogarty, C. E., et al. (2016). "Extracellular Reactive Oxygen Species Drive Apoptosis-Induced Proliferation via  
795 *Drosophila* Macrophages." *Curr Biol* **26**(5): 575-584.
- 796 26. Fox, D. T., et al. (2020). "Model systems for regeneration: *Drosophila*." *Development* **147**(7).
- 797 27. Fuchs, Y. and H. Steller (2015). "Live to die another way: modes of programmed cell death and the signals  
798 emanating from dying cells." *Nat Rev Mol Cell Biol* **16**(6): 329-344.
- 799 28. Gong, T., et al. (2020). "DAMP-sensing receptors in sterile inflammation and inflammatory diseases." *Nat Rev*  
800 *Immunol* **20**(2): 95-112.
- 801 29. Gordon, O., et al. (2018). "alpha-actinin accounts for the bioactivity of actin preparations in inducing STAT  
802 target genes in *Drosophila melanogaster*." *Elife* **7**.
- 803 30. Grasl-Kraupp, B., et al. (1995). "In situ detection of fragmented DNA (TUNEL assay) fails to discriminate  
804 among apoptosis, necrosis, and autolytic cell death: a cautionary note." *Hepatology* **21**(5): 1465-1468.
- 805 31. Hajibabaie, F., et al. (2023). "Types of Cell Death from a Molecular Perspective." *Biology (Basel)* **12**(11).
- 806 32. Hakkarainen, T. W., et al. (2014). "Necrotizing soft tissue infections: review and current concepts in treatment,  
807 systems of care, and outcomes." *Curr Probl Surg* **51**(8): 344-362.
- 808 33. Hariharan, I. K. and F. Serras (2017). "Imaginal disc regeneration takes flight." *Curr Opin Cell Biol* **48**: 10-16.
- 809 34. Harris, R. E. (2023). "Investigating Tissue Regeneration Using the DUAL Control Genetic Ablation System."  
810 *Methods Mol Biol* **2599**: 255-270.
- 811 35. Harris, R. E., et al. (2020). "Damage-responsive, maturity-silenced enhancers regulate multiple genes that  
812 direct regeneration in *Drosophila*." *Elife* **9**.
- 813 36. Hay, B. A., et al. (1994). "Expression of baculovirus P35 prevents cell death in *Drosophila*." *Development*  
814 **120**(8): 2121-2129.
- 815 37. Herrera, S. C. and E. A. Bach (2019). "JAK/STAT signaling in stem cells and regeneration: from *Drosophila* to  
816 vertebrates." *Development* **146**(2).
- 817 38. Huh, J. R., et al. (2004). "Compensatory proliferation induced by cell death in the *Drosophila* wing disc  
818 requires activity of the apical cell death caspase Dronc in a nonapoptotic role." *Curr Biol* **14**(14): 1262-1266.

- 819 39. Jaiswal, J., et al. (2023). "Mutual repression between JNK/AP-1 and JAK/STAT stratifies senescent and  
820 proliferative cell behaviors during tissue regeneration." *PLoS Biol* **21**(5): e3001665.
- 821 40. Jung, Y., et al. (2010). "Signals from dying hepatocytes trigger growth of liver progenitors." *Gut* **59**(5): 655-  
822 665.
- 823 41. Kamber Kaya, H. E., et al. (2017). "An inhibitory mono-ubiquitylation of the Drosophila initiator caspase Dronc  
824 functions in both apoptotic and non-apoptotic pathways." *PLoS Genet* **13**(2): e1006438.
- 825 42. Karsch-Bluman, A., et al. (2019). "Tissue necrosis and its role in cancer progression." *Oncogene* **38**(11):  
826 1920-1935.
- 827 43. Katsuyama, T., et al. (2015). "During Drosophila disc regeneration, JAK/STAT coordinates cell proliferation  
828 with Dilp8-mediated developmental delay." *Proc Natl Acad Sci U S A* **112**(18): E2327-2336.
- 829 44. Khan, S. J., et al. (2017). "The Drosophila Duox maturation factor is a key component of a positive feedback  
830 loop that sustains regeneration signaling." *PLoS Genet* **13**(7): e1006937.
- 831 45. Kim, J., et al. (1996). "Integration of positional signals and regulation of wing formation and identity by  
832 Drosophila vestigial gene." *Nature* **382**(6587): 133-138.
- 833 46. Klemm, J., et al. (2021). "Necrosis-induced apoptosis promotes regeneration in Drosophila wing imaginal  
834 discs." *Genetics* **219**(3).
- 835 47. Konstantinidis, K., et al. (2012). "Mechanisms of cell death in heart disease." *Arterioscler Thromb Vasc Biol*  
836 **32**(7): 1552-1562.
- 837 48. La Fortezza, M., et al. (2016). "JAK/STAT signalling mediates cell survival in response to tissue stress."  
838 *Development* **143**(16): 2907-2919.
- 839 49. La Marca, J. E. and H. E. Richardson (2020). "Two-Faced: Roles of JNK Signalling During Tumourigenesis in  
840 the Drosophila Model." *Front Cell Dev Biol* **8**: 42.
- 841 50. Ledru, M., et al. (2022). "Differential gene expression analysis identified determinants of cell fate plasticity  
842 during radiation-induced regeneration in Drosophila." *PLoS Genet* **18**(1): e1009989.
- 843 51. Li, F., et al. (2010). "Apoptotic cells activate the "phoenix rising" pathway to promote wound healing and tissue  
844 regeneration." *Sci Signal* **3**(110): ra13.
- 845 52. Li, M., et al. (2019). "Characterization of TNF-induced cell death in Drosophila reveals caspase- and JNK-  
846 dependent necrosis and its role in tumor suppression." *Cell Death Dis* **10**(8): 613.
- 847 53. Li, Z., et al. (2023). "Advances in experimental models of osteonecrosis of the femoral head." *J Orthop*  
848 *Translat* **39**: 88-99.
- 849 54. Liu, K., et al. (2013). "Modeling calcium-overload mediated necrosis in Drosophila." *Methods Mol Biol* **1004**:  
850 203-213.
- 851 55. Madigan, J. P., et al. (2002). "DNA double-strand break-induced phosphorylation of Drosophila histone variant  
852 H2Av helps prevent radiation-induced apoptosis." *Nucleic Acids Res* **30**(17): 3698-3705.
- 853 56. Martin, R., et al. (2017). "Distinct regenerative potential of trunk and appendages of Drosophila mediated by  
854 JNK signalling." *Development* **144**(21): 3946-3956.
- 855 57. Masi, L., et al. (2007). "Osteonecrosis in genetic disorders." *Clin Cases Miner Bone Metab* **4**(1): 27-29.

- 856 58. Meier, P., et al. (2000). "The Drosophila caspase DRONC is regulated by DIAP1." *EMBO J* **19**(4): 598-611.
- 857 59. Ming, M., et al. (2014). "Persephone/Spatzle pathogen sensors mediate the activation of Toll receptor
- 858 signaling in response to endogenous danger signals in apoptosis-deficient Drosophila." *J Biol Chem* **289**(11):
- 859 7558-7568.
- 860 60. Morata, G., et al. (2011). "Mitogenic signaling from apoptotic cells in Drosophila." *Dev Growth Differ* **53**(2):
- 861 168-176.
- 862 61. Mulay, S. R., et al. (2016). "Necroinflammation in Kidney Disease." *J Am Soc Nephrol* **27**(1): 27-39.
- 863 62. Nakada, H., et al. (2019). "Fat necrosis after breast-conserving oncoplastic surgery." *Breast Cancer* **26**(1):
- 864 125-130.
- 865 63. Nano, M. and D. J. Montell (2024). "Apoptotic signaling: Beyond cell death." *Semin Cell Dev Biol* **156**: 22-34.
- 866 64. Nishida, H., et al. (2024). "Necrosensor: a genetically encoded fluorescent sensor for visualizing necrosis in
- 867 Drosophila." *Biol Open* **13**(1).
- 868 65. Pellettieri, J., et al. (2010). "Cell death and tissue remodeling in planarian regeneration." *Dev Biol* **338**(1): 76-
- 869 85.
- 870 66. Perez-Garijo, A. (2018). "When dying is not the end: Apoptotic caspases as drivers of proliferation." *Semin*
- 871 *Cell Dev Biol* **82**: 86-95.
- 872 67. Perez-Garijo, A., et al. (2004). "Caspase inhibition during apoptosis causes abnormal signalling and
- 873 developmental aberrations in Drosophila." *Development* **131**(22): 5591-5598.
- 874 68. Perez-Garijo, A., et al. (2005). "Dpp signaling and the induction of neoplastic tumors by caspase-inhibited
- 875 apoptotic cells in Drosophila." *Proc Natl Acad Sci U S A* **102**(49): 17664-17669.
- 876 69. Perez-Garijo, A., et al. (2009). "The role of Dpp and Wg in compensatory proliferation and in the formation of
- 877 hyperplastic overgrowths caused by apoptotic cells in the Drosophila wing disc." *Development* **136**(7): 1169-1177.
- 878 70. Perez-Garijo, A. and H. Steller (2015). "Spreading the word: non-autonomous effects of apoptosis during
- 879 development, regeneration and disease." *Development* **142**(19): 3253-3262.
- 880 71. Pinal, N., et al. (2019). "Pro-apoptotic and pro-proliferation functions of the JNK pathway of Drosophila: roles
- 881 in cell competition, tumorigenesis and regeneration." *Open Biol* **9**(3): 180256.
- 882 72. Pinal, N., et al. (2018). "Short-term activation of the Jun N-terminal kinase pathway in apoptosis-deficient cells
- 883 of Drosophila induces tumorigenesis." *Nature Communications* **9**(1).
- 884 73. Robertson, S. A., et al. (2017). "Mastectomy skin flap necrosis: challenges and solutions." *Breast Cancer*
- 885 *(Dove Med Press)* **9**: 141-152.
- 886 74. Roh, J. S. and D. H. Sohn (2018). "Damage-Associated Molecular Patterns in Inflammatory Diseases."
- 887 *Immune Netw* **18**(4): e27.
- 888 75. Ryoo, H. D. and A. Bergmann (2012). "The role of apoptosis-induced proliferation for regeneration and
- 889 cancer." *Cold Spring Harb Perspect Biol* **4**(8): a008797.
- 890 76. Ryoo, H. D., et al. (2004). "Apoptotic cells can induce compensatory cell proliferation through the JNK and the
- 891 Wingless signaling pathways." *Dev Cell* **7**(4): 491-501.

- 892 77. Schott, S., et al. (2017). "A fluorescent toolkit for spatiotemporal tracking of apoptotic cells in living *Drosophila*  
893 tissues." *Development* **144**(20): 3840-3846.
- 894 78. Shapiro, P. J., et al. (2008). "Regulation of the *Drosophila* apoptosome through feedback inhibition." *Nat Cell*  
895 *Biol* **10**(12): 1440-1446.
- 896 79. Shinoda, N., et al. (2019). "Dronc-independent basal executioner caspase activity sustains *Drosophila*  
897 imaginal tissue growth." *Proc Natl Acad Sci U S A* **116**(41): 20539-20544.
- 898 80. Siegrist, S. E., et al. (2010). "Inactivation of both Foxo and reaper promotes long-term adult neurogenesis in  
899 *Drosophila*." *Curr Biol* **20**(7): 643-648.
- 900 81. Su, T. T. (2020). "Non-apoptotic roles of apoptotic proteases: new tricks for an old dog." *Open Biol* **10**(8):  
901 200130.
- 902 82. Tonnus, W., et al. (2021). "The role of regulated necrosis in endocrine diseases." *Nat Rev Endocrinol* **17**(8):  
903 497-510.
- 904 83. Tseng, A. S., et al. (2007). "Apoptosis is required during early stages of tail regeneration in *Xenopus laevis*."  
905 *Dev Biol* **301**(1): 62-69.
- 906 84. Venereau, E., et al. (2015). "DAMPs from Cell Death to New Life." *Front Immunol* **6**: 422.
- 907 85. Verghese, S. and T. T. Su (2016). "*Drosophila* Wnt and STAT Define Apoptosis-Resistant Epithelial Cells for  
908 Tissue Regeneration after Irradiation." *PLoS Biol* **14**(9): e1002536.
- 909 86. Verghese, S. and T. T. Su (2018). "Ionizing radiation induces stem cell-like properties in a caspase-dependent  
910 manner in *Drosophila*." *PLoS Genet* **14**(11): e1007659.
- 911 87. Vríz, S., et al. (2014). "Cell death: a program to regenerate." *Curr Top Dev Biol* **108**: 121-151.
- 912 88. Wang, L. H. and N. E. Baker (2019). "Salvador-Warts-Hippo pathway regulates sensory organ development  
913 via caspase-dependent nonapoptotic signaling." *Cell Death Dis* **10**(9): 669.
- 914 89. Worley, M. I. and I. K. Hariharan (2022). "Imaginal Disc Regeneration: Something Old, Something New." *Cold*  
915 *Spring Harb Perspect Biol* **14**(11).
- 916 90. Worley, M. I., et al. (2012). "Regeneration and transdetermination in *Drosophila* imaginal discs." *Annu Rev*  
917 *Genet* **46**: 289-310.
- 918 91. Wu, M. Y., et al. (2018). "Current Mechanistic Concepts in Ischemia and Reperfusion Injury." *Cell Physiol*  
919 *Biochem* **46**(4): 1650-1667.
- 920 92. Xu, D., et al. (2005). "The CARD-carrying caspase Dronc is essential for most, but not all, developmental cell  
921 death in *Drosophila*." *Development* **132**(9): 2125-2134.
- 922 93. Yang, X., et al. (2021). "Treatment of Radiation-Induced Brain Necrosis." *Oxid Med Cell Longev* **2021**:  
923 4793517.
- 924 94. Yang, Y., et al. (2013). "Neuronal necrosis and spreading death in a *Drosophila* genetic model." *Cell Death*  
925 *Dis* **4**: e723.
- 926

927 **Article and author information**

928 **Jacob Klemm**

929 School of Life Sciences, Arizona State University, Life Sciences E (LSE) 354, 427 Tyler Mall, Tempe,  
930 Arizona, 85287-4501

931 [jwklemm@asu.edu](mailto:jwklemm@asu.edu)

932 ORCID iD: 0000-0002-1414-5089

933

934 **Chloe Van Hazel**

935 School of Life Sciences, Arizona State University, Life Sciences E (LSE) 354, 427 Tyler Mall, Tempe,  
936 Arizona, 85287-4501

937

938 **Robin Harris**

939 School of Life Sciences, Arizona State University, Life Sciences E (LSE) 354, 427 Tyler Mall, Tempe,  
940 Arizona, 85287-4501

941 **For correspondence:** [reharri4@asu.edu](mailto:reharri4@asu.edu)

942 ORCID iD: 0000-0001-6945-6741

943

944 **Figure Legends**

945 **Figure 1. The NiA response is restricted to pouch cells following ablation.** (A) A schematic of the  
946  $DC^{GluR1}$  ablation scheme. This system utilizes a split LexA transcriptional activator that promotes the  
947 expression of *lexAop-GluR1* following a short heat shock (45 min at 37°C). (B) A schematic of the different  
948 tissue domains and compartments targeted for  $GAL4/UAS/GAL80^{ts}$  ( $GAL4^{ts}$ ) ablation. (C) A schematic of the  
949 temperature scheme used to induce necrosis with  $GAL4^{ts}>GluR1$  following the heat shift (20 hr at 30°C)  
950 induced inactivation of  $GAL80^{ts}$ . (D) A control disc for DUAL Control ( $DC^{NA}$ ) experiments bearing *lexAop-*  
951 *GFP*, which labels the domain targeted for ablation with  $DC^{GluR1}$ . (E) A  $DC^{GluR1}$  ablated disc at 18 hr of  
952 regeneration bearing *lexAop-GFP*, yellow arrowheads indicate pouch NiA, red arrowhead indicates a cluster  
953 of Dcp-1-positive cells in the posterior pleura. (F) A control disc for  $R85E08-GAL4^{ts}$  ( $R85^{ts}>GFP$ ) ablation.  
954 (G) An  $R85E08^{ts}>GluR1,GFP$  ablated disc, arrowheads indicate the presence of NiA cells following ablation.  
955 (H) A control disc for whole pouch ( $rn^{ts}>GFP$ ) ablation. (I-J) A  $rn^{ts}>GluR1,GFP$  ablated disc dissected  
956 immediately following the downshift (0 hr, I) and after 24 hr of regeneration (R24, J). (K) A control disc for  
957 notum ablation ( $pnr^{ts}>GFP$ ). (L-M)  $pnr^{ts}>GluR1,GFP$  ablated discs at 0 hr (L) and 24 hr (M), open  
958 arrowheads highlight the absence of the Wg notum stripe following ablation. (N) A control disc for hinge  
959 ablation ( $R73G07ts>GFP$ ). (O-P)  $R73G08^{ts}>GluR1,GFP$  ablated discs at 0 hr (O) and 24 hr (P). Open  
960 arrowhead in (O) indicates the absence of NiA in the adjacent wing pouch. (Q) A control disc for posterior  
961 compartment ablation ( $hh^{ts}>GFP$ ). (R-S')  $hh^{ts}>GluR1,GFP$  ablated discs at 0 hr (R-R') and 24 hr (S-S').  
962 Dotted lines in (R') and (S') show an absence of NiA in the anterior hinge. (T) A quantification of the NiA  
963 response in the anterior pouch, hinge, and notum in control (n= 13), 0 hr (n= 14), and 24 hr (n= 12) discs in  
964 response to *hh* ablation. NiA are defined as Dcp-1-positive (Dcp-1+ve), GFP-negative (GFP-ve) cells. See  
965 Supplementary Genotypes file for exact genotypes.

966

967 **Figure 1 – figure supplement 1.** (A) A *nub<sup>ts</sup>>GluR1,GFP* ablated disc at 0 hr. (B) A *DC<sup>GluR1</sup>* ablated disc  
968 highlighting the overlap between wound edge apoptosis and the JNK target Mmp1 (arrowhead). (C) A  
969 control disc for anterior compartment ablation (*ptc<sup>ts</sup>>RFP*). (D-E') *ptc<sup>ts</sup>>GluR1,RFP* ablated discs at 0 hr (D-  
970 D') and 24 hr (E-E'). Dotted lines in (D') and (E') highlight the lack of NiA cells in the hinge. (F) A  
971 quantification of the NiA response to *ptc* ablation in the pouch, hinge, and notum of control (n= 14), 0 hr (n=  
972 15), and 24 hr (n= 14) discs, with NiA being defined as Dcp-1-positive (+ve), RFP-negative (-ve) cells. (G) A  
973 control disc for *FLP/FRT* clonal ablation, where *actin-FRT>stop>FRT-GAL-4 (act<sup>ts</sup>>>RFP)* drives the  
974 expression of *UAS-RFP* in clonal patches of cells after a short heat shock (see materials and methods for  
975 details). (H-H'') A wing disc with clonal patches of *UAS-RFP*, *UAS-GluR1* expressing cells. (H') is a zoom-in  
976 of pouch and hinge clones with arrowheads pointing to NiA cells, while (H'') is a zoom-in of notum clones. (I)  
977 A quantification of the number of NiA cells induced following ablation with *act<sup>ts</sup>>>GluR1* (n= 11),  
978 *R85E08<sup>ts</sup>>GluR1* (n= 10), *ptc<sup>ts</sup>>GluR1* (n= 15), and *hh<sup>ts</sup>>GluR1* (n= 14), highlighting that NiA number  
979 increases with increasing area of ablation. See Supplementary Genotypes file for exact genotypes.  
980

981 **Figure 2. NiA formation in pouch cells is regulated by the Wg and JAK/STAT pathways. (A).** A control  
982 disc ( $DC^{NA}$ ) bearing the  $10xSTAT-GFP$  reporter, showing the hinge-specific Stat92E activity that is normally  
983 absent from the wing pouch. **(B)** A  $DC^{GluR1}$  ablated disc bearing  $10xSTAT-GFP$ . Following damage, pouch-  
984 specific reporter expression is observed at high levels at the wound edge (arrowhead) and low levels at the  
985 NiA area of the pouch (open arrowhead). **(C-E)**  $DC^{GluR1}>>y^{RNAi}$  **(C, n=14)** versus  $DC^{GluR1}>>dome^{RNAi}$  **(D,**  
986  $n=14)$  ablated discs, with the number of Dcp-1+ve cells in the WE vs LP quantified in **(E)**,  $P^{****} < 0.0001$ .  
987 Data were analyzed with a one-way ANOVA followed by a multiple comparisons test. **(F)** A  $DC^{GluR1}hh-GAL4$   
988 ablation schematic ( $DC^{GluR1}hh^{ts}$ ). A short heat shock (45 min at 37°C) induces split  $LexA/lexAop-GluR1$   
989 ablation, while a heat shift (18 hr at 30°C) following the heat shock will inactivate  $GAL80^{ts}$  and permit  $UAS-X$   
990 expression. **(G)** A  $DC^{GluR1}hh^{ts}>GFP$  ablated disc, where GFP highlights the area of the disc being targeted  
991 for JAK/STAT and Wg knockdown in the following experiments. The posterior NiA will be assayed in  
992 response to knockdown while anterior NiA serve as an internal control. **(H)** A control  $hh^{ts}>GFP,Stat92E^{RNAi}$   
993 disc showing no changes in cell death. **(I)** A  $DC^{GluR1}hh^{ts}>Stat92E^{RNAi}$  ablated disc, arrowhead highlights an  
994 increase in pouch NiA. **(J)** A control  $DC^{NA}$  disc showing developmental Wg expression. **(K)** A  $DC^{GluR1}>>y^{RNAi}$   
995 ablated disc showing that NiA cells avoid the areas of the pouch with high Wg expression, while wound edge  
996 apoptotic cells overlap the developmental and damage-specific Wg-expressing cells (arrowhead). **(L)** A  
997 control  $hh^{ts}>GFP,wg^{RNAi}$  disc showing the absence of Wg in the posterior pouch and no change in posterior  
998 cell death. **(M)** A  $DC^{GluR1}hh^{ts}>wg^{RNAi}$  ablated disc with NiA cells observed at the posterior margin  
999 (arrowhead) while anterior NiA avoid the Wg margin stripe (open arrowhead). See Supplementary  
1000 Genotypes file for exact genotypes.

1001

1002 **Figure 2 – figure supplement 1. (A)** A  $DC^{NA}>>hop48A$  control disc with high levels of Dcp-1 observed  
1003 throughout the pouch. **(B)** A  $DC^{GluR1}>>hop48A$  ablated disc with high levels of apoptosis throughout the  
1004 pouch, likely due to  $UAS-hop48A$  expression **(A)**. **(C)** A  $DC^{GluR1}hh^{ts}>GFP$  ablated disc with nubbin and  
1005 DCAD highlighting the ablated *salm* domain and GFP labeling the area of  $UAS-X$  expression. **(D)** A control  
1006  $hh^{ts}>GFP,Zfh2^{RNAi}$  disc showing no changes in cell death. **(E)** A  $DC^{GluR1}hh^{ts}>Zfh2^{RNAi}$  ablated disc showing a  
1007 slight increase in pouch NiA. **(F)** A control disc bearing the *vgQE-lacZ* reporter showing the area of the  
1008 pouch with vestigial quadrant enhancer expression. **(G)** A  $DC^{GluR1}$  ablated disc bearing *vgQE-lacZ*, showing  
1009 the high degree of overlap between NiA cells and lacZ-expressing cells. **(H)** A control  $hh^{ts}>Wg$  disc with no  
1010 strong changes in cell death observed. **(I)** A  $DC^{GluR1}hh^{ts}>Wg$  ablated disc showing an increase in apoptosis  
1011 across the wing pouch and in the posterior pleura. See Supplementary Genotypes file for exact genotypes.  
1012

1013 **Figure 3. NiA promotes proliferation late in regeneration. (A-A''')** A time course of  $DC^{GluR1}$  ablated discs  
1014 bearing the *PCNA-GFP* reporter at 18 hr (A), 24 hr (A'), 36 hr (A''), and 48 hr (A'''). (B-B''') A time course  
1015 of  $DC^{GluR1} >> y^{RNAi}$  ablated discs at 18 hr (B), 24 hr (B'), 36 hr (B''), and 48 hr (B'''). High levels of EdU are  
1016 observed by 36 hr that remain elevated at 48 hr. (C-C''') A time course of  $DC^{hepCA} >> y^{RNAi}$  ablated discs at 18  
1017 hr (C), 24 hr (C'), 36 hr (C''), and 48 hr (C'''). (D-D''') A time course of  $DC^{GluR1} >> mir(RHG)$  ablated discs at  
1018 18 hr (D), 24 hr (D'), 36 hr (D''), and 48 hr (D'''). (E) A graph of the  $DC^{GluR1}$ ,  $DC^{hepCA}$ , and  $DC^{NA}$  EdU time  
1019 courses highlight the pattern of EdU labeling in the wing pouch between each system. (F) A quantification of  
1020 EdU signal intensity between  $DC^{GluR1} >> y^{RNAi}$  at 18 hr (n= 10), 24 hr (n= 10), 36 hr (n= 10), 48 hr (n= 10), and  
1021  $DC^{GluR1} >> mir(RHG)$  at 18 hr (n= 10), 24 hr (n= 8), 36 hr (n= 11), and 48 hr (n= 10) time courses, ns, not  
1022 significant; \*\*\*P = 0.0002; \*\*\*\*P <0.0001; data were analyzed with a one-way ANOVA and multiple  
1023 comparisons test. (G-J)  $DC^{GluR1}$  ablated discs with different populations of apoptotic cells suppressed by  
1024 *mir(RHG)*. (G) A control  $DC^{GluR1} >> y^{RNAi}$  ablated disc showing the typical pattern of NiA formation. (H) A  
1025  $DC^{GluR1} >> mir(RHG)$  ablated disc suppressing both wound edge apoptosis and NiA cells. (I) A  
1026  $DC^{GluR1} >> miRHG; DR^{WNT}-GAL80$  ablated disc, which targets the LP for *UAS-mir(RHG)* expression  
1027 (*LP > mir(RHG)*). (J) A  $DC^{GluR1} \times R85E08 > mir(RHG)$  ablated disc, which targets the WE for suppression  
1028 (*WE > mir(RHG)*). The dotted lines each panel highlight the area of *UAS-mir(RHG)* expression. (K-N)  $DC^{GluR1}$   
1029 ablated discs with representative EdU labels at R36 in response to  $y^{RNAi}$  (K), whole-pouch *mir(RHG)* (L),  
1030 *LP > mir(RHG)* (M), and *WE > mir(RHG)* (N). (O) A quantification of the normalized EdU fluorescent intensity  
1031 of  $DC^{GluR1} >> y^{RNAi}$  18 hr (n= 10),  $DC^{GluR1} >> y^{RNAi}$  36 hr (n= 10),  $DC^{GluR1} >> mir(RHG)$  36 hr (n= 11),  
1032 *LP > mir(RHG)* 36 hr (n= 10), and *WE > mir(RHG)* 36 hr (n= 9) ablated discs; \*P = 0.0189, \*\*P = 0.0044, \*\*\*P =  
1033 0.0008, \*\*\*\*P < 0.0001; data were analyzed with a one-way ANOVA and multiple comparisons tests. LP =  
1034 lateral pouch, WE = wound edge. See Supplementary Genotypes file for exact genotypes.

1035

1036 **Figure 3 – figure supplement 1. (A-A''')** A  $DC^{NA}>>y^{RNAi}$  control time course at 18 hr (**A**), 24 hr (**A'**), 36 hr  
1037 (**A''**), and 48 hr (**A'''**). The folds of the wing pouch were used to outline the EdU signal for quantification in all  
1038 experiments, as visualized by DAPI. (**B-C**) A  $DC^{NA}>>y^{RNAi}$  control disc (**B**) with EdU labeling relative to a  
1039  $DC^{NA}>>mir(RHG)$  control disc (**C**). (**D**) A quantification of discs in (**B**, n=10) and (**C**, n=10) demonstrating  
1040 that miRHG expression does not alter EdU levels, ns, not significant. Data were analyzed with a Student's T-  
1041 test. See Supplementary Genotypes file for exact genotypes.  
1042

1043 **Figure 4 NiA promote proliferation independent of Apoptosis-induced Proliferation (AiP).** (A-A') A  
1044  $DC^{NA}$  control disc bearing the *wg-lacZ* reporter. (B-B') A  $DC^{GluR1}$  ablated disc with *wg-lacZ* showing the  
1045 expression of the reporter during regeneration, with lacZ-expressing cells at the wound edge. The 24 hr time  
1046 point was chosen as an intermediate between NiA formation (18 hr) and blastema formation (36 hr), when  
1047 secreted factors are likely to be detected. (C-C') A  $DC^{GluR1}>>P35$  ablated disc bearing *wg-lacZ* with lac-Z  
1048 expressing cells observed at the WE (arrowhead) but not in the LP (open arrowhead). (D-D') A  $DC^{NA}$  control  
1049 disc bearing the *dpp-lacZ* reporter. (E-E') A  $DC^{GluR1}$  ablated disc with *dpp-lacZ*, with lac-Z expressing cells  
1050 observed at the WE. (F-F') A  $DC^{GluR1}>>P35$  ablated disc bearing *dpp-lacZ*, with lacZ expressing cells at the  
1051 WE (arrowhead) but not the LP (open arrowhead). (G) A  $DC^{GluR1}$  ablated disc bearing the transcriptional *AP-*  
1052 *1-GFP* reporter and labeled with dihydroethidium (DHE). Low levels of DHE labeling are observed at the  
1053 WE, where AP-1-GFP expression occurs (arrowhead), while no DHE labeling is observed in the LP. (H) A  
1054  $DC^{GluR1}>>Cat,Sod1$  ablated disc showing reduced WE apoptosis (open arrowhead) but no change in NiA  
1055 formation. (I) A  $DC^{GluR1}>>DuoX^{RNAi}$  ablated disc showing a similar pattern to (H) with an observed loss of WE  
1056 apoptosis (open arrowhead) but no change in NiA formation. (J-L)  $DC^{GluR1}$  ablated discs bearing *yRNAi* (J),  
1057 *P35* (K), and *LP>P35* (L) at 36 hr and labeled with EdU. (M) A quantification of discs in (J-L) demonstrate  
1058 no change in EdU labeling upon the expression of P35 in the LP (*LP>P35*, L), confirming that NiA promote  
1059 proliferation independent of AiP, ns, not significant. Data were analyzed with a one-way ANOVA followed by  
1060 a multiple comparisons test. LP = lateral pouch, AiP = apoptosis-induced proliferation. See Supplementary  
1061 Genotypes file for exact genotypes.  
1062

1063 **Figure 4 – figure supplement 1.** (A) A  $DC^{NA}$  control disc bearing the *spi-lacZ* reporter, showing no lacZ  
1064 expression in the wing disc. (B) A  $DC^{GluR1}>>P35$  ablated disc bearing *spi-lacZ* showing a few lac-Z-  
1065 expressing cells at the WE. (C) A  $DC^{NA}$  control disc bearing *mol-lacZ* highlighting the developmental  
1066 expression pattern of *mol* in the wing disc. (D) A  $DC^{GluR1}$  ablated disc bearing *mol-lacZ*, with a slight  
1067 increase in lacZ expression observed at the WE (arrowhead). See Supplementary Genotypes file for exact  
1068 genotypes.  
1069

1070 **Figure 5. NiCP cells persist in the disc proper throughout regeneration. (A-D)** A time course of  $DC^{GluR1}$   
1071 ablated discs bearing the fluorescent caspase reporter  $UAS-GC3Ai$  at 18 hr (A), 24 hr (B), 36 hr (C), and 48  
1072 hr (D). (E) A  $DC^{GluR1}>>GC3Ai$  ablated disc at 64 hr, with GC3Ai-positive cells present at the WE after the  
1073 nubbin marker is reestablished (arrowhead). (F-F') A  $DC^{GluR1}>>GC3Ai$  ablated disc at 36 hr with GC3Ai-  
1074 positive cells associated with the mitotic PH3 marker. Yellow arrowhead in (F') points to cytoplasmic,  
1075 undisturbed cells, while the red arrowhead points to cells with a pyknotic morphology. (G-H) A  $DC^{GluR1}$   
1076  $LP>GC3Ai$  ablated disc at 18 hr (G) and 36 hr (H). The arrowhead in (H) highlights the presence of GC3Ai-  
1077 labeled NiA cells at the WE. (I-I') A  $DC^{hepCA}>>GC3Ai$  ablated disc at 18 hr with apoptotic cells present  
1078 throughout the disc proper. (J-J') A  $DC^{hepCA}>>GC3Ai$  ablated disc at 36 hr (J) and 64 hr (J'); all apoptotic  
1079 cells appear to be pushed out towards the basal surface of the disc proper. (K-K') A  $DC^{GluR1}>>GC3Ai$   
1080 ablated discs at 18 hr with NiA cells present in the disc proper. (L-L') A  $DC^{GluR1} LP>GC3Ai$  ablated disc at  
1081 36 hr, with columnar-shaped GC3Ai-positive cells in the disc proper (yellow arrowhead) alongside pyknotic,  
1082 rounded GC3Ai-positive cells (red arrowhead), showing that there are a mix of morphologically apoptotic NiA  
1083 and non-apoptotic NiCP cells in the disc proper. See Supplementary Genotypes file for exact genotypes.  
1084

1085 **Figure 5 – figure supplement 1. (A)** A  $DC^{NA}>GC3Ai$  control disc driving  $UAS-GC3Ai$  in the pouch, HA  
1086 labels all  $GC3Ai$ -expressing cells, while the cells with activated  $GC3Ai$  also have green fluorescence. **(B)** A  
1087  $DC^{GluR1}>>GC3Ai$  ablated disc showing  $GC3Ai$ -positive NiA cells and, to a lesser extent,  $GC3Ai$ -positive WE  
1088 apoptotic cells. **(C)** A  $DC^{GluR1} LP>GC3Ai$  ablated disc, with HA highlighting the restricted expression of  
1089  $GC3Ai$  to the LP, thus excluding WE cells. **(D-E)**  $DC^{GluR1}$  ablated discs at 18 hr **(D)** and 36 hr **(E)** with  
1090  $GC3Ai/TUNEL$  double-positive NiA at both time points. **(F-G)**  $DC^{GluR1}$  ablated discs at 18 hr **(F)** and 36 hr **(G)**  
1091 showing strong overlap between NiA and  $yH2Av$  at 18 hr (arrowheads in **F**) that diminishes by 36 hr (open  
1092 arrowheads in **G**). See Supplementary Genotypes file for exact genotypes.  
1093

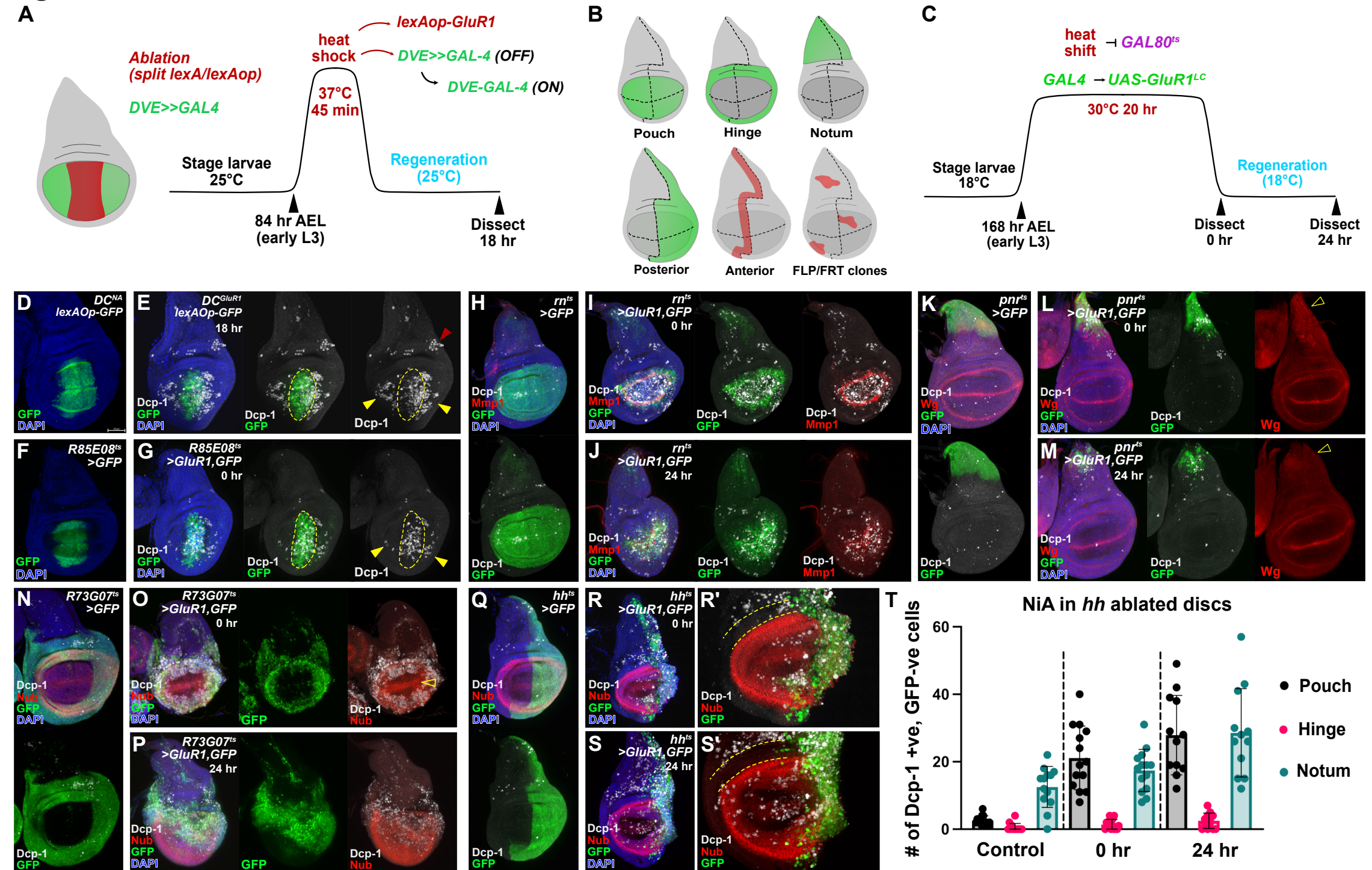
1094 **Figure 6 – NiCP have sublethal levels of activated effector caspases. (A-A')** A  $DC^{GluR1} DBS-GFP$   
1095 ablated disc at 18 hr showing strong overlap between Dcp-1 and  $DBS-GFP$ -positive NiA/NiCP. **(B-B''')**  
1096  $DC^{GluR1} CasEx^{ts}>G-trace$  ablated discs at 18 hr with RFP labeled WE cells, (arrowhead), but no RFP or  
1097 lineage trace-positive labeling is observed in NiA/NiCP (open arrowheads). **(C)** A  $DC^{hepCA} CasEx^{ts}>G-trace$   
1098 ablated disc at 18 hr showing a high level of overlap between apoptotic cells and both RFP and the lineage  
1099 trace (arrowhead). **(D-E)**  $DC^{GluR1} CasEx>GFP$  ablated discs at 18 hr **(D)** and 36 hr **(E)** showing that  
1100 NiA/NiCP are labeled by *CasExpress* in a sensitized background. See Supplementary Genotypes file for  
1101 exact genotypes.  
1102

1103 **Figure 6 – figure supplement 1. (A)** A  $DC^{GluR1} CasEx^{ts} > G\text{-trace}$  ablated disc at 36 hr with no lineage-  
1104 positive NiA/NiCP, despite the presence of clonal patches of cells traced by developmental caspase activity.  
1105 See Supplementary Genotypes file for exact genotypes.  
1106

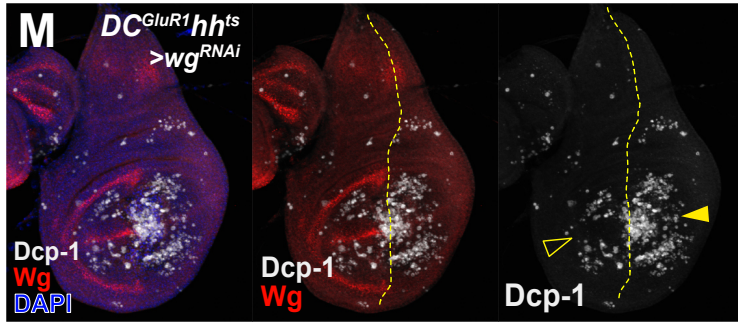
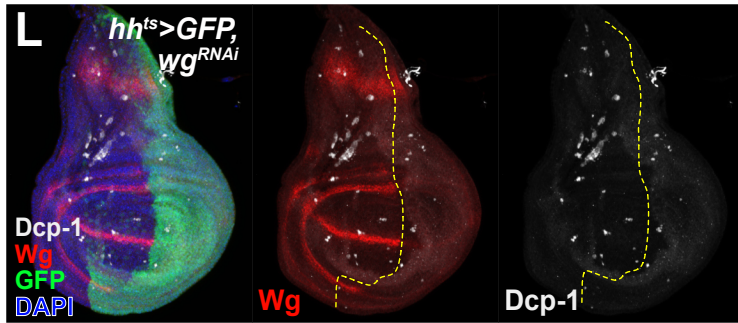
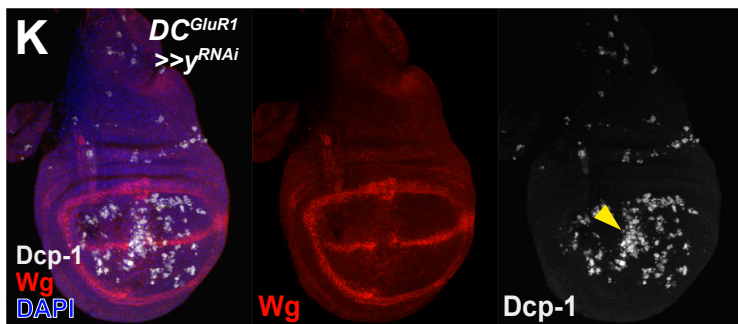
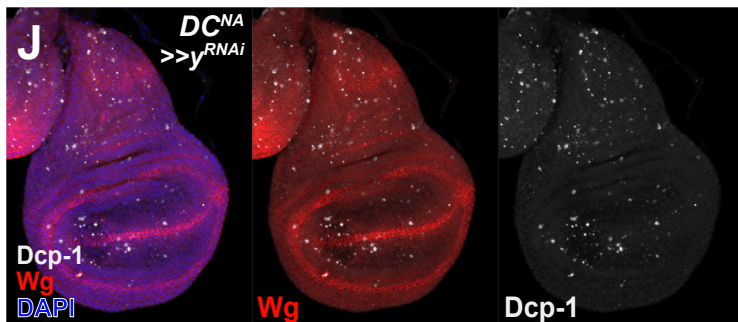
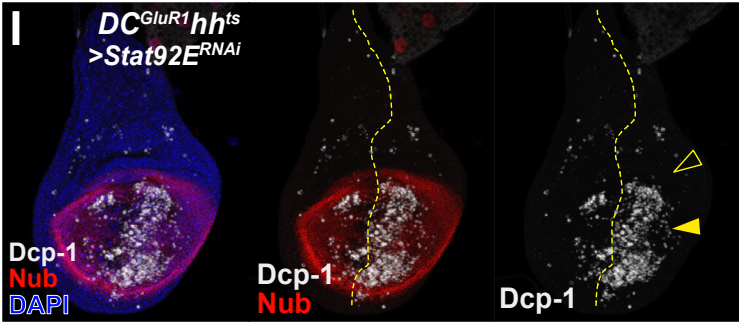
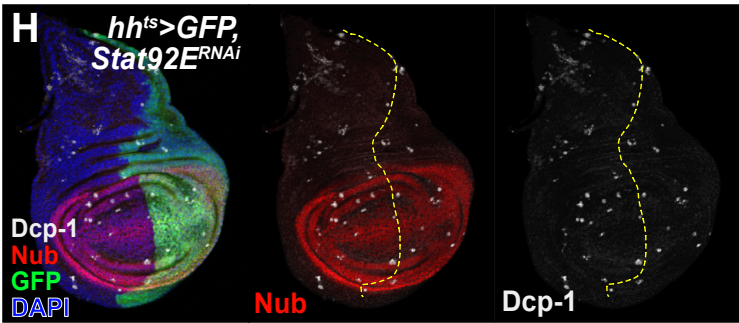
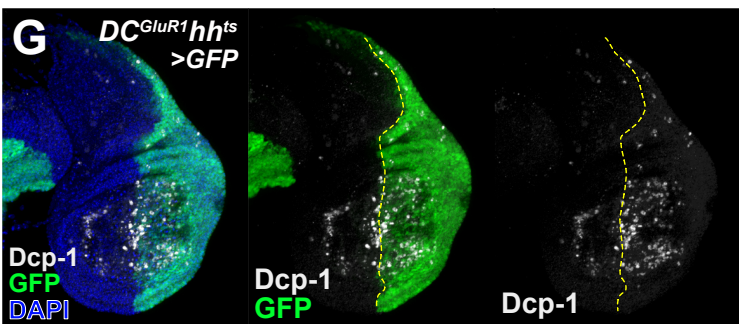
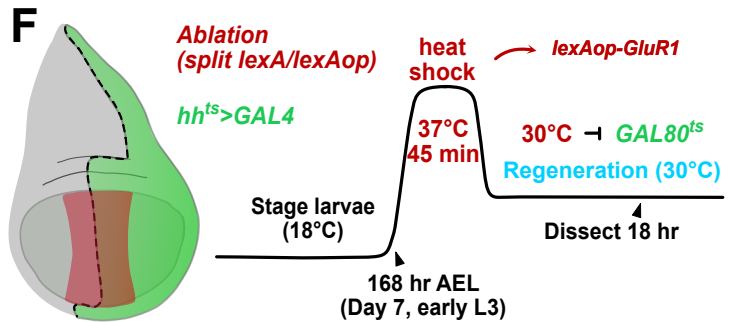
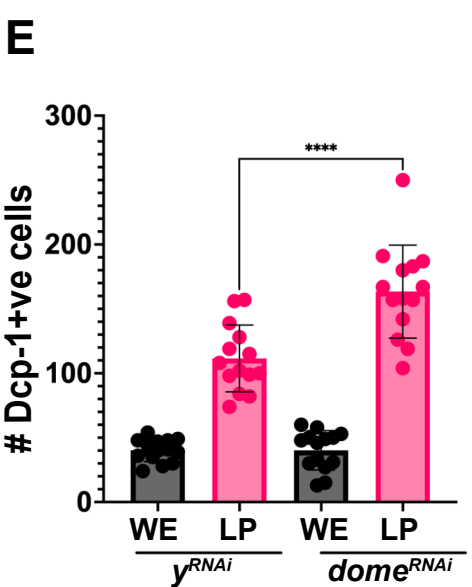
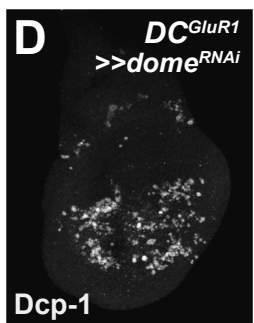
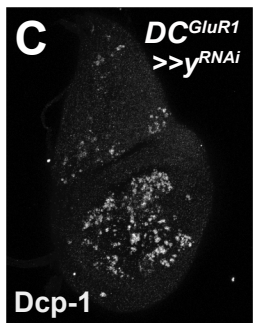
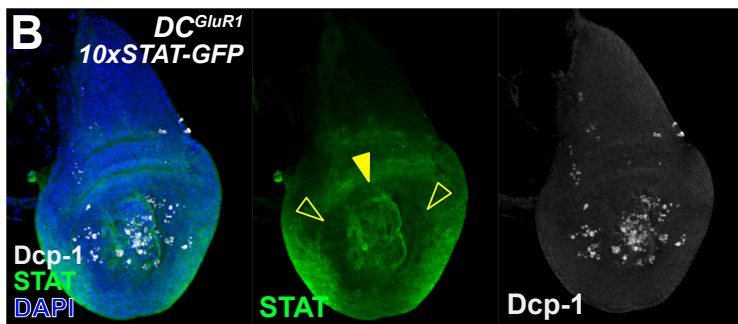
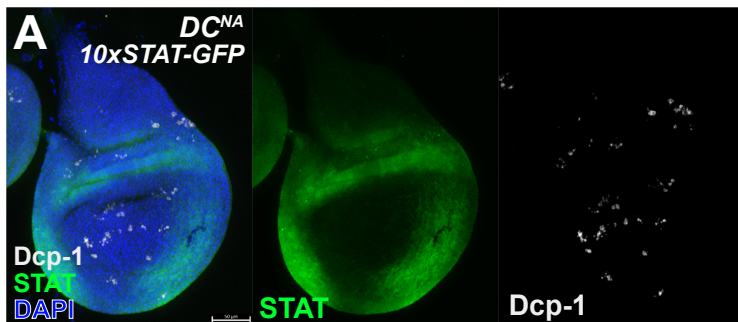
1107 **Figure 7 – Dronc activity in NiCP promotes regeneration. (A-J)** Representative  $DC^{GluR1}$  ablated discs at  
1108 18 hr **(A,C,E,G and I)** with Dcp-1 and Mmp1 labeling, and at 36 hr **(B,D,F,H and J)** with EdU labeling,  
1109 bearing  $UAS-y^{RNAi}$  **(A-B)**,  $UAS-mir(RHG)$  **(C-D)**,  $Dronc^{I29/+}$  **(E-F)**,  $UAS-Dronc^{DN}$  **(G-H)**, or  $UAS-DIAP1$  **(I-J)**.  
1110 Open arrowhead in **(F)** indicates a strong reduction in EdU labeling. Open arrowheads in **(I)** show a strong  
1111 suppression of NiA/NiCP as detected by Dcp-1. **(K)** A quantification of NiA/NiCP number (Dcp-1+ve, Mmp1-  
1112 ve cells) in  $UAS-y^{RNAi}$  (n = 11),  $UAS-mir(RHG)$  (n = 8),  $Dronc^{I29/+}$  (n = 10),  $UAS- UAS-Dronc^{DN}$  (n = 7), and  
1113  $UAS-DIAP1$  (n = 8), ns, not significant,  $P^{****} < 0.0001$ . Data were analyzed with a one-way ANOVA followed  
1114 by a multiple comparisons test. **(L)** A quantification of EdU fluorescence intensity with  $UAS-y^{RNAi}$  (n = 20),  
1115  $UAS-mir(RHG)$  (n = 14),  $Dronc^{I29/+}$  (n = 18)  $UAS- UAS-Dronc^{DN}$  (n = 17) and  $DIAP1$  (n = 10), ns, not  
1116 significant,  $P^{***} = 0.0004$ ,  $P^{****} < 0.0001$ . Data were analyzed with a one-way ANOVA followed by a multiple  
1117 comparisons test. **(M)** Regeneration scoring of  $DC^{GluR1}$  ablated flies in a +/+ versus a  $Dronc^{I29/+}$  background.  
1118 Representative images for regenerated +/+ (left) and  $Dronc^{I29/+}$  are shown above the graph. **(N)** A diagram  
1119 depicting the three different caspase-positive cell types that occur following necrotic ablation. Following  
1120 necrosis, JNK signaling at the WE promotes Dronc activation, which mediates WE apoptosis and  
1121 proliferation through the AiP feed forward loop. In the LP, some DAMP-like signal(s) leads to the formation  
1122 of necrosis-induced apoptosis (NiA), which undergo apoptotic death resulting from high levels of Dronc,  
1123 Dcp-1 and Drice activity, and necrosis-induced caspase positive (NiCP) cells that utilize Dronc to promote  
1124 proliferation and subsequent regeneration independent of both JNK and AiP signaling. Both WE apoptosis  
1125 and NiCP act to promote regeneration through independent mechanisms of Dronc-mediated regenerative  
1126 proliferation. See Supplementary Genotypes file for exact genotypes.  
1127

1128 **Figure 7 – figure supplement 1. (A)** A quantification of regenerated wing size in an unablated control  
1129 ( $DC^{NA}$ ) wildtype (+/+, males = 17, females = 11) and  $Dronc^{I29}/+$  (males = 11, females = 22) background, and  
1130 following  $DC^{GluR1}$  ablation in a +/+ (n = 16 males, n = 19 females) and  $Dronc^{I29}/+$  (n = 19 males, n = 28  
1131 females) background, ns = not significant,  $P^{***} = 0.0001$ , data were analyzed with a one-way ANOVA  
1132 followed by a multiple comparisons test. See Supplementary Genotypes file for exact genotypes.  
1133 Representative images for regenerated +/+ (top) and  $Dronc^{I29}/+$  (bottom) wings are shown to the right of the  
1134 graph. See Supplementary Genotypes file for exact genotypes.  
1135

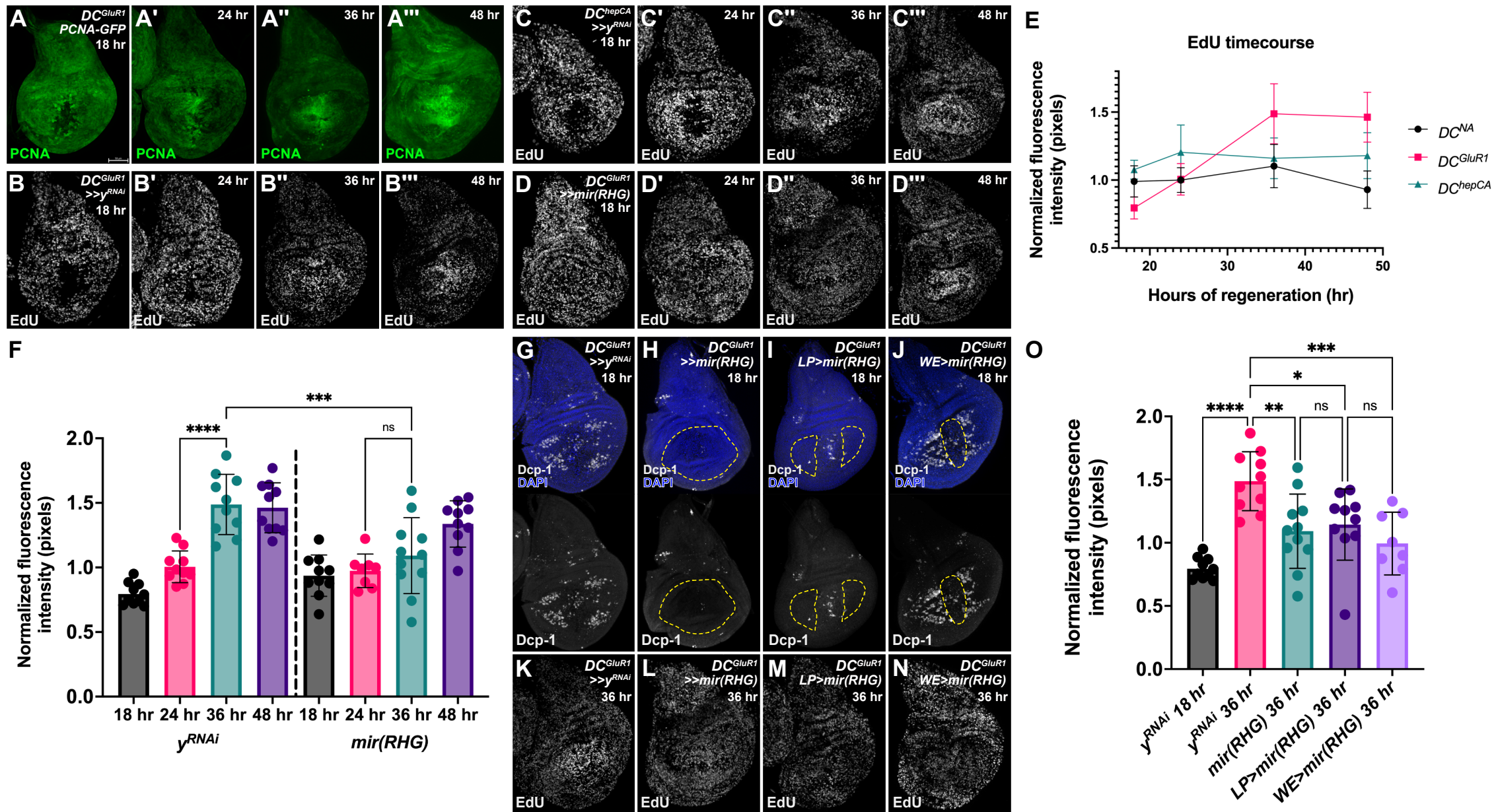
# Figure 1



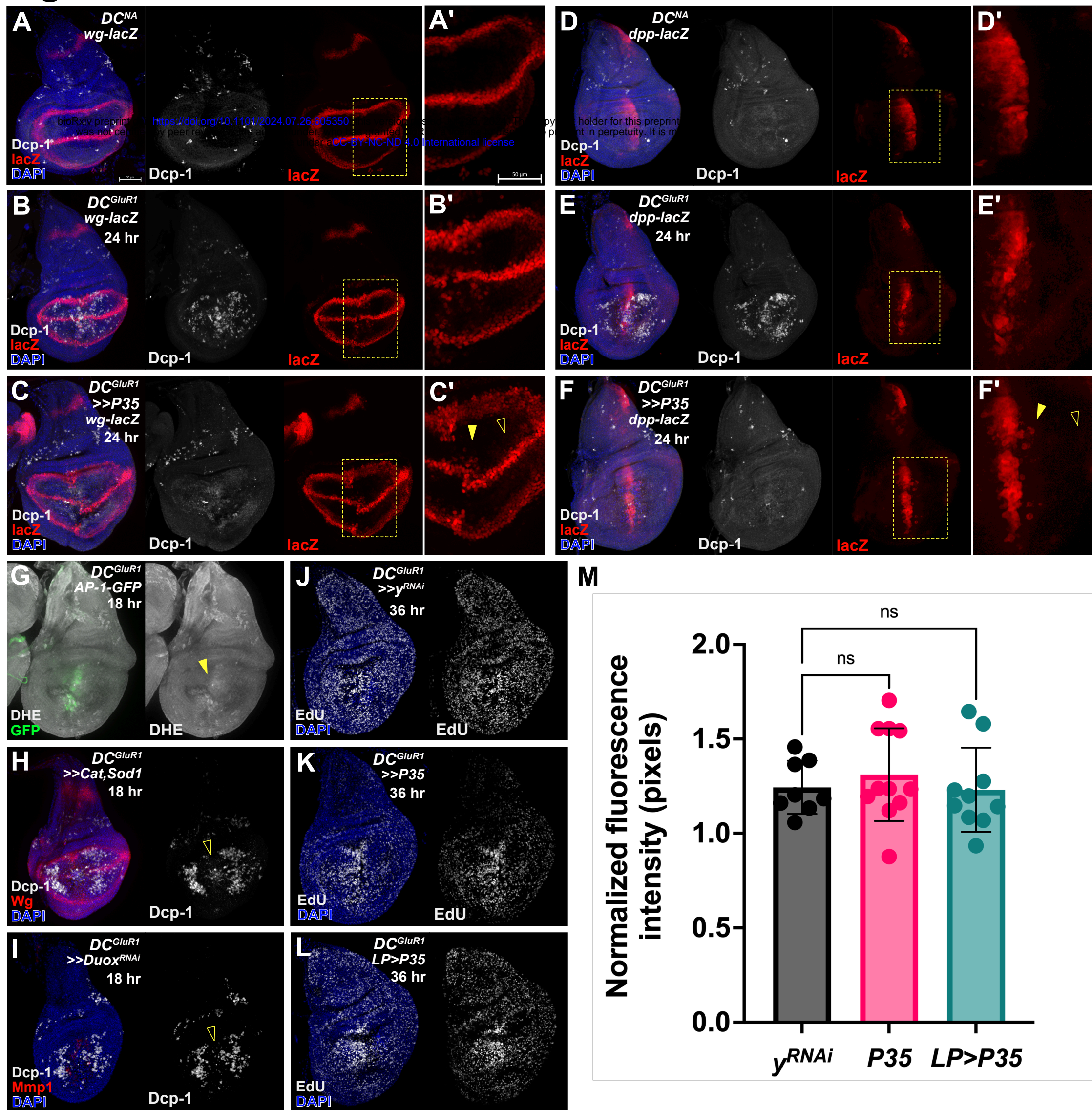
# Figure 2

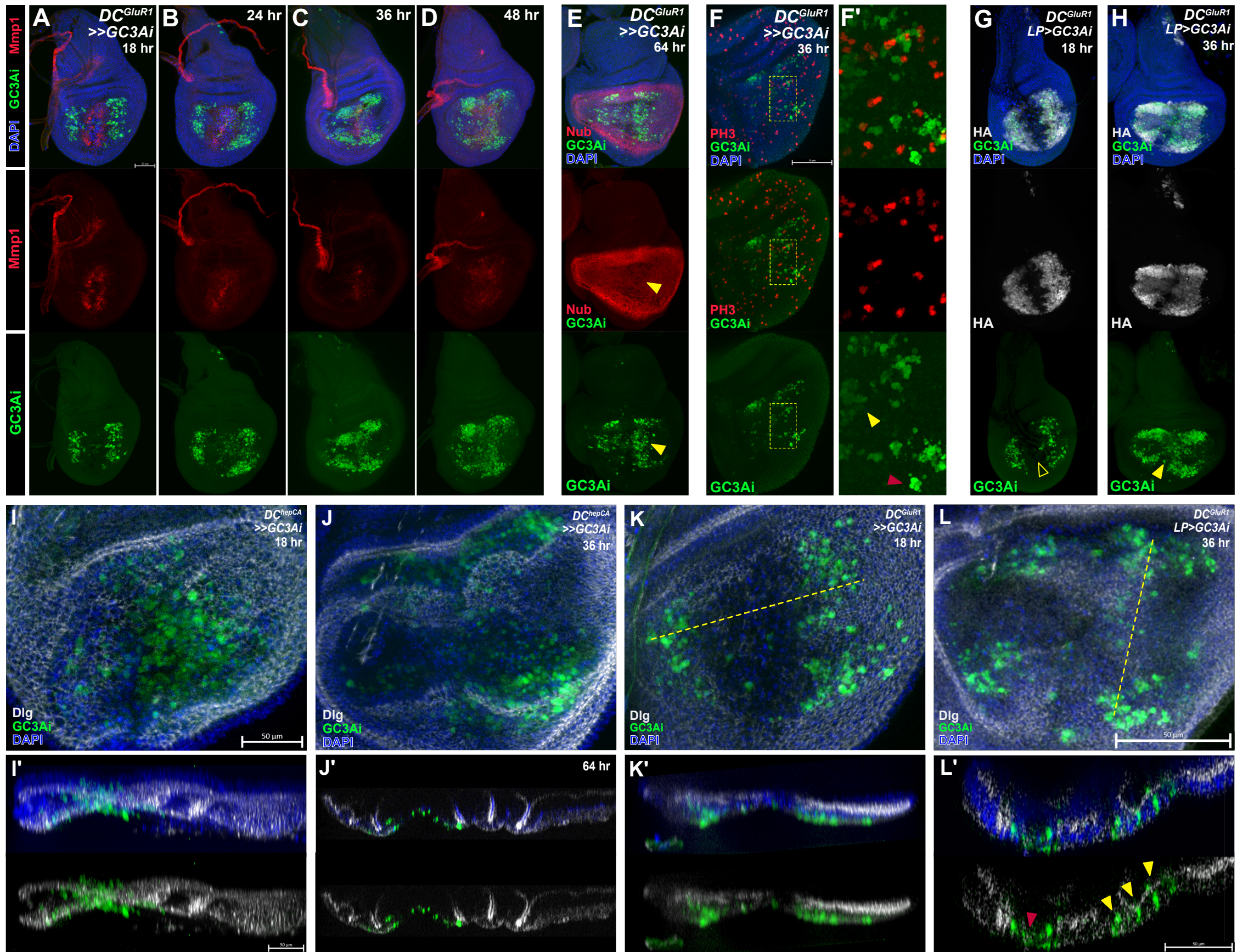


# Figure 3



# Figure 4



**Figure 5**

# Figure 6

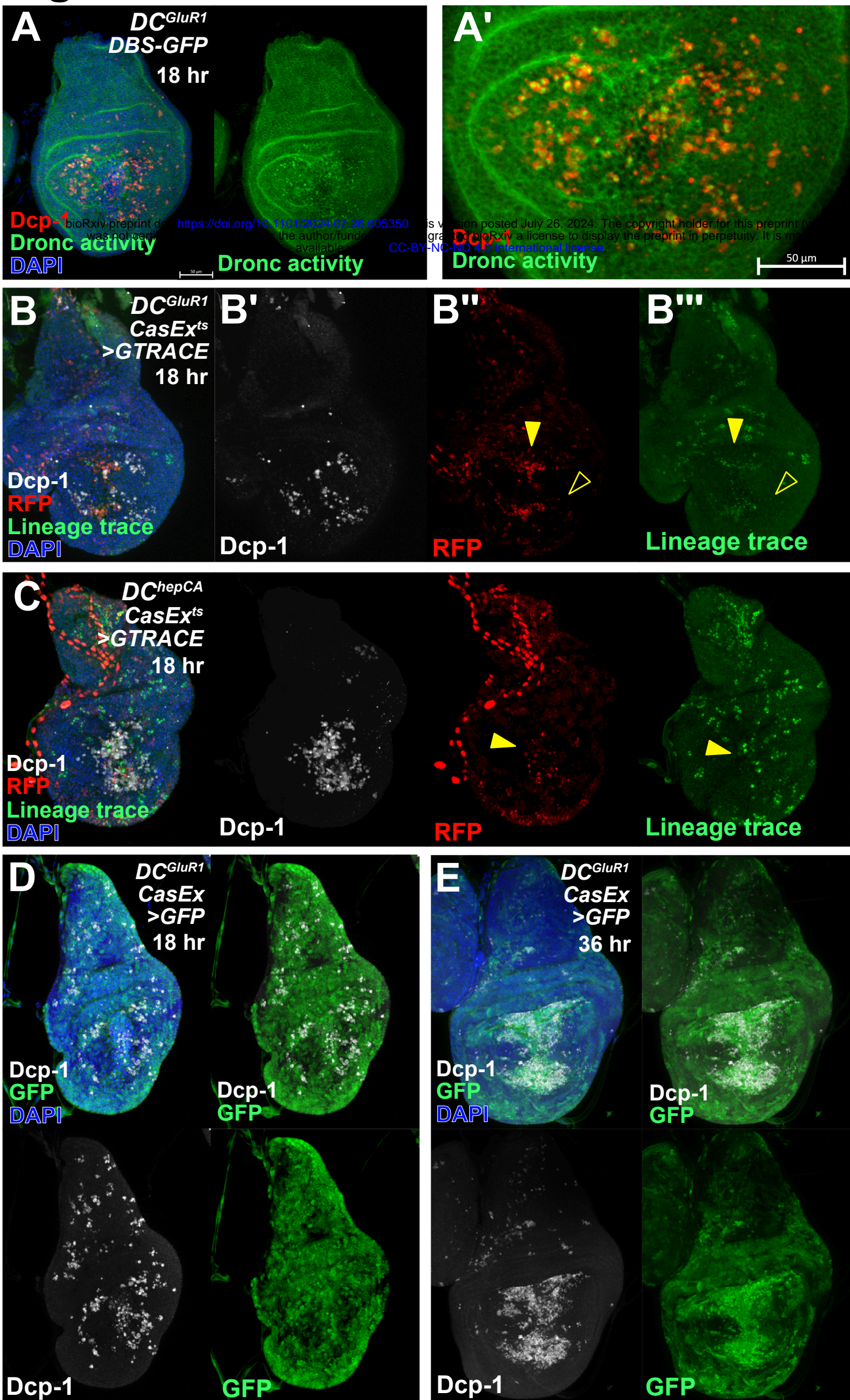


# Figure 7

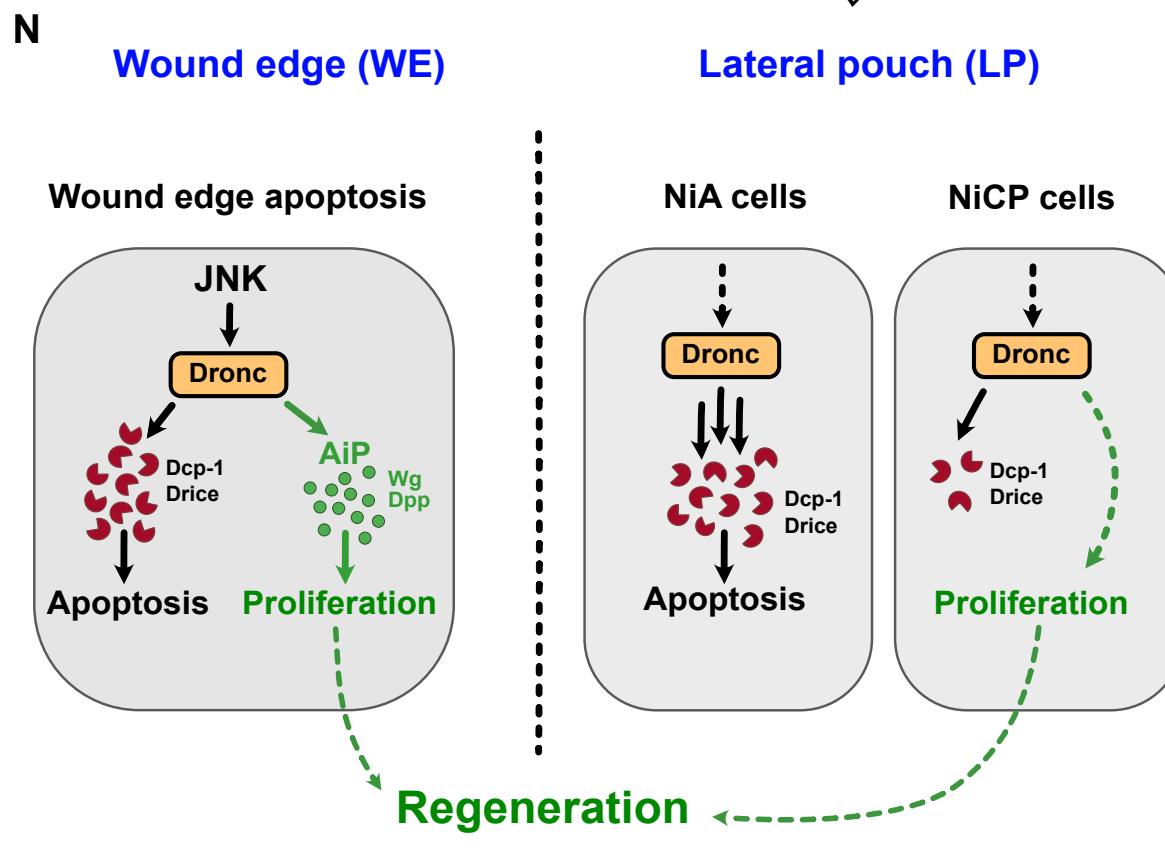
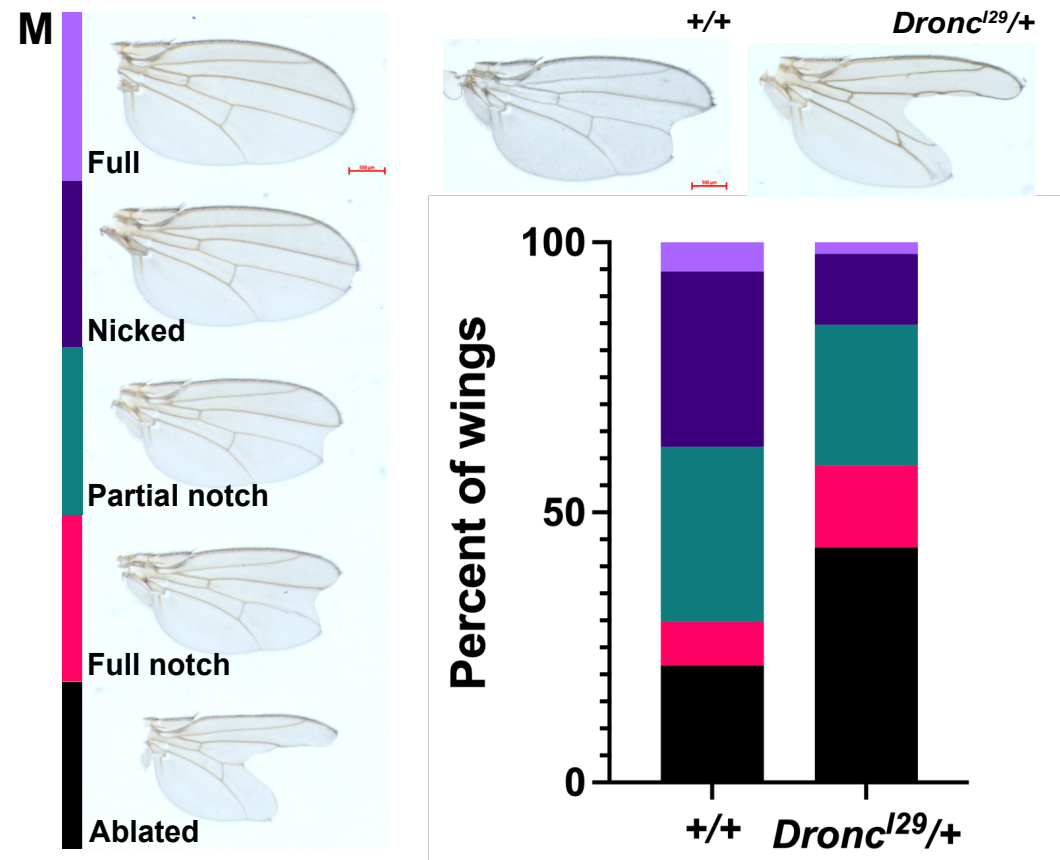
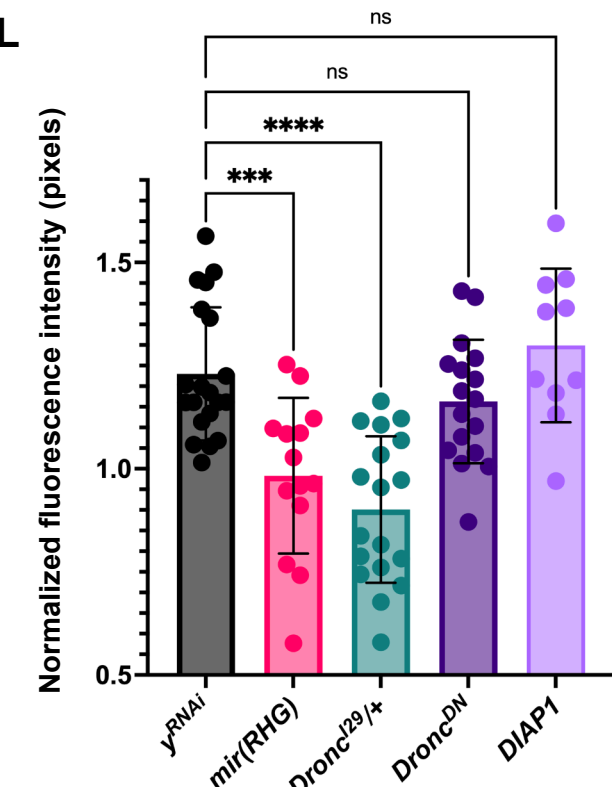
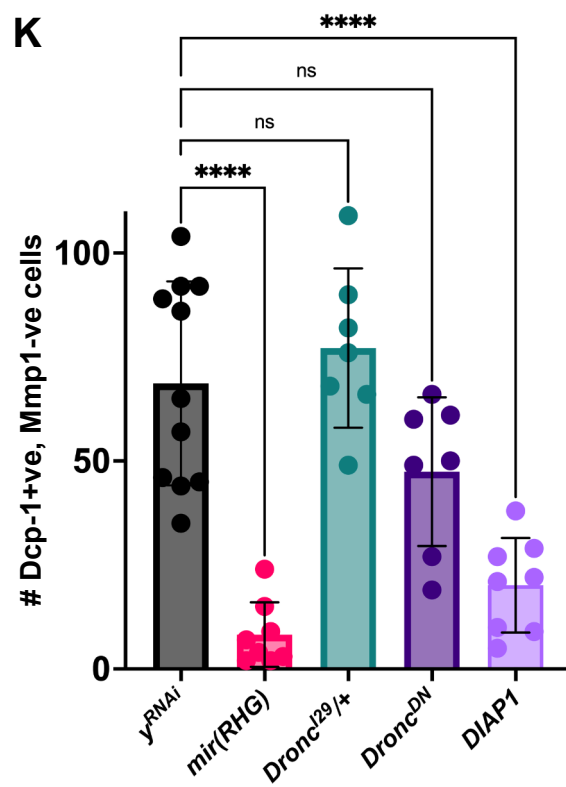
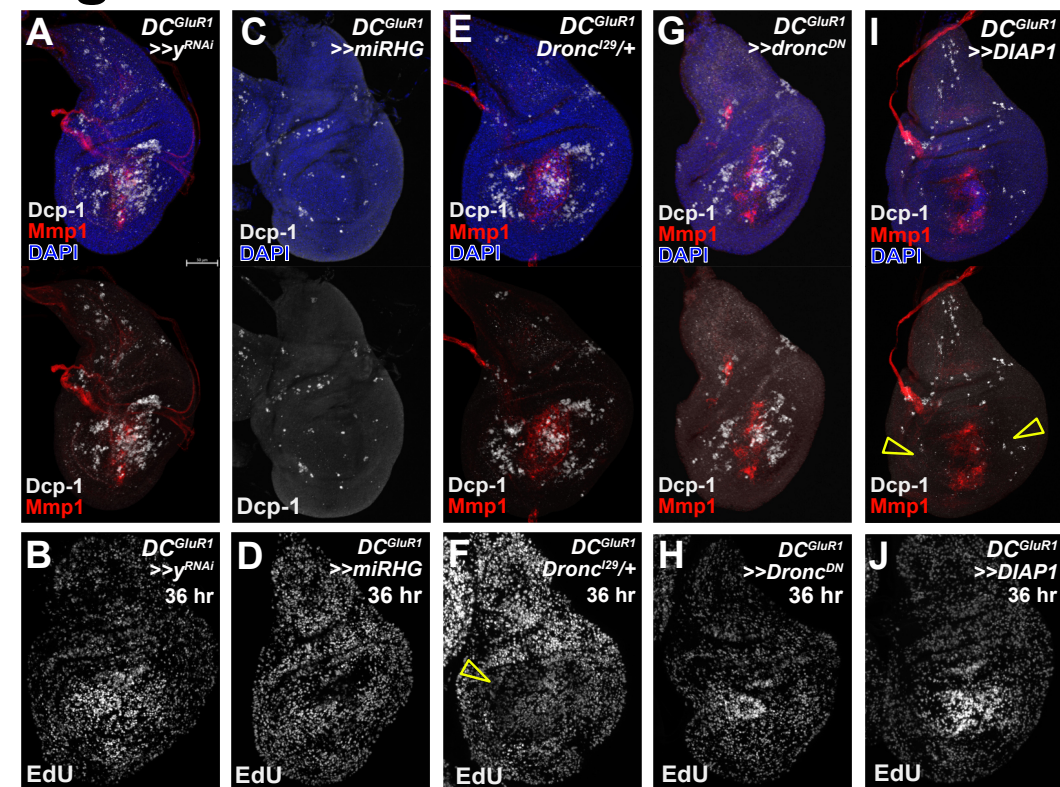


# Figure S1

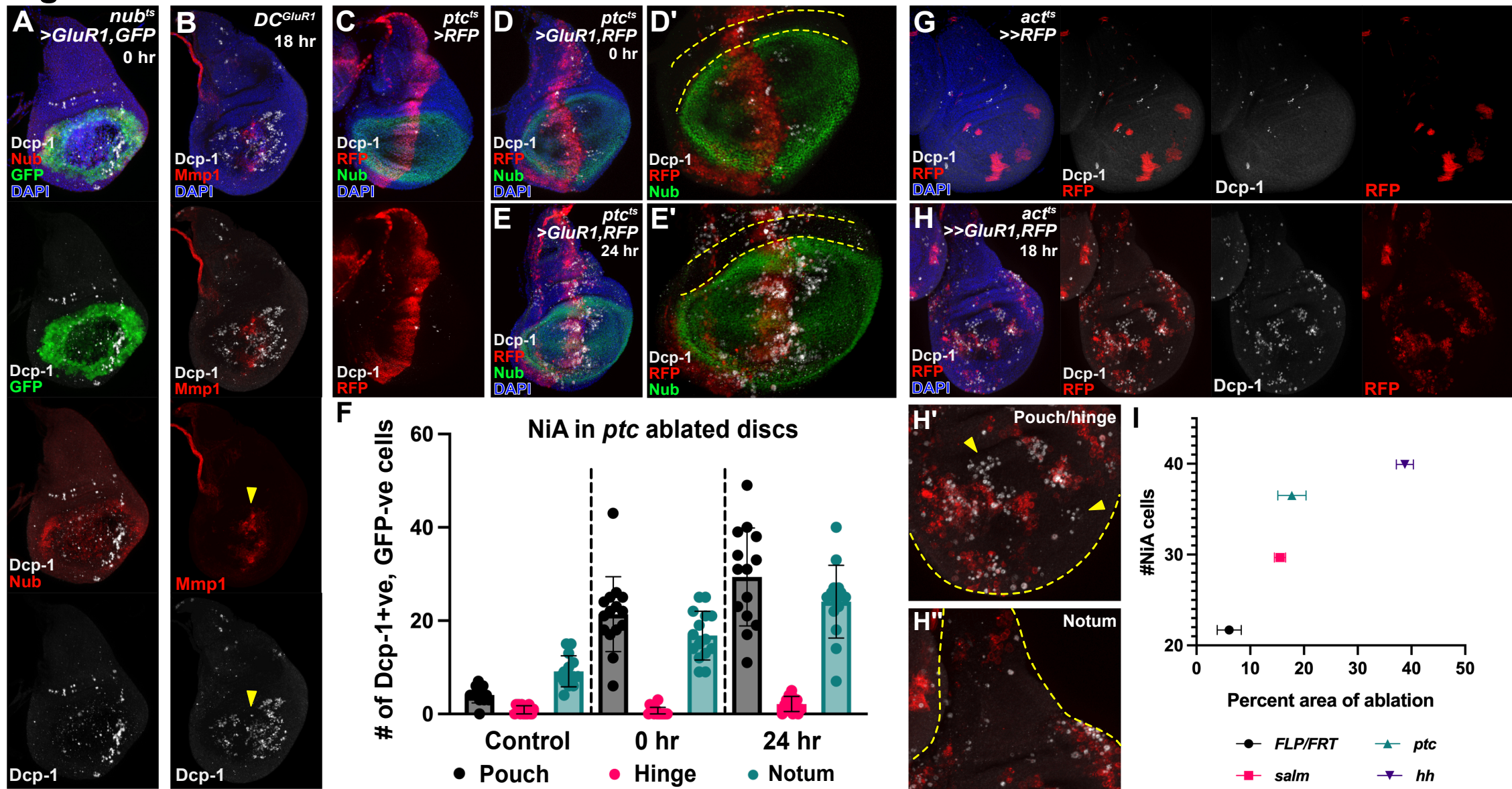


# Figure S2

bioRxiv preprint doi: <https://doi.org/10.1101/2024.07.26.605350>; this version posted July 26, 2024. The copyright holder for this preprint (which was not certified by peer review) is the author/funder, who has granted bioRxiv a license to display the preprint in perpetuity. It is made available under aCC-BY-NC-ND 4.0 International license.

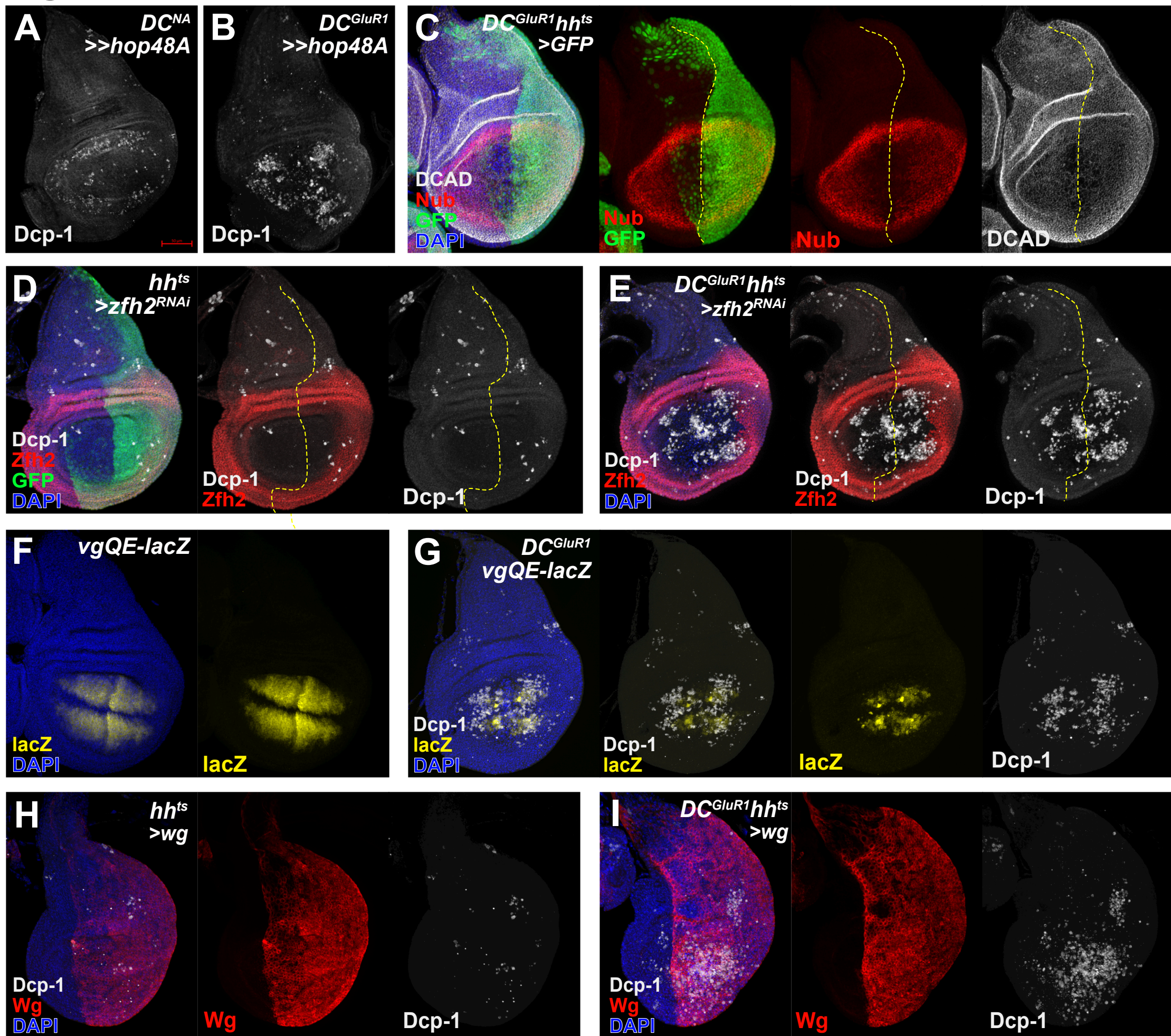
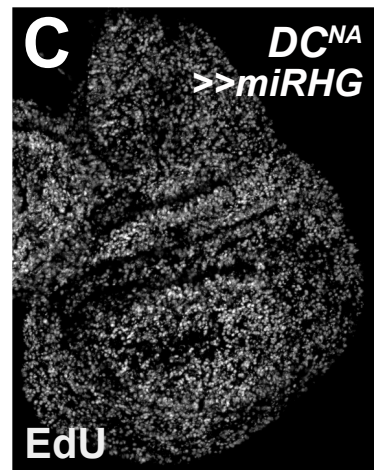
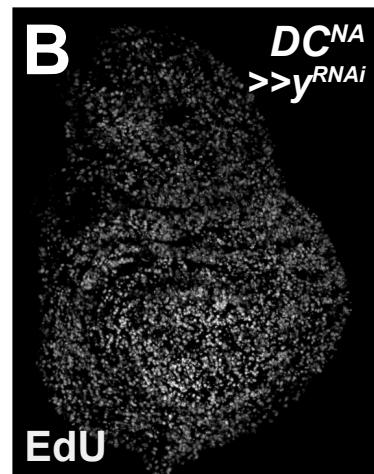
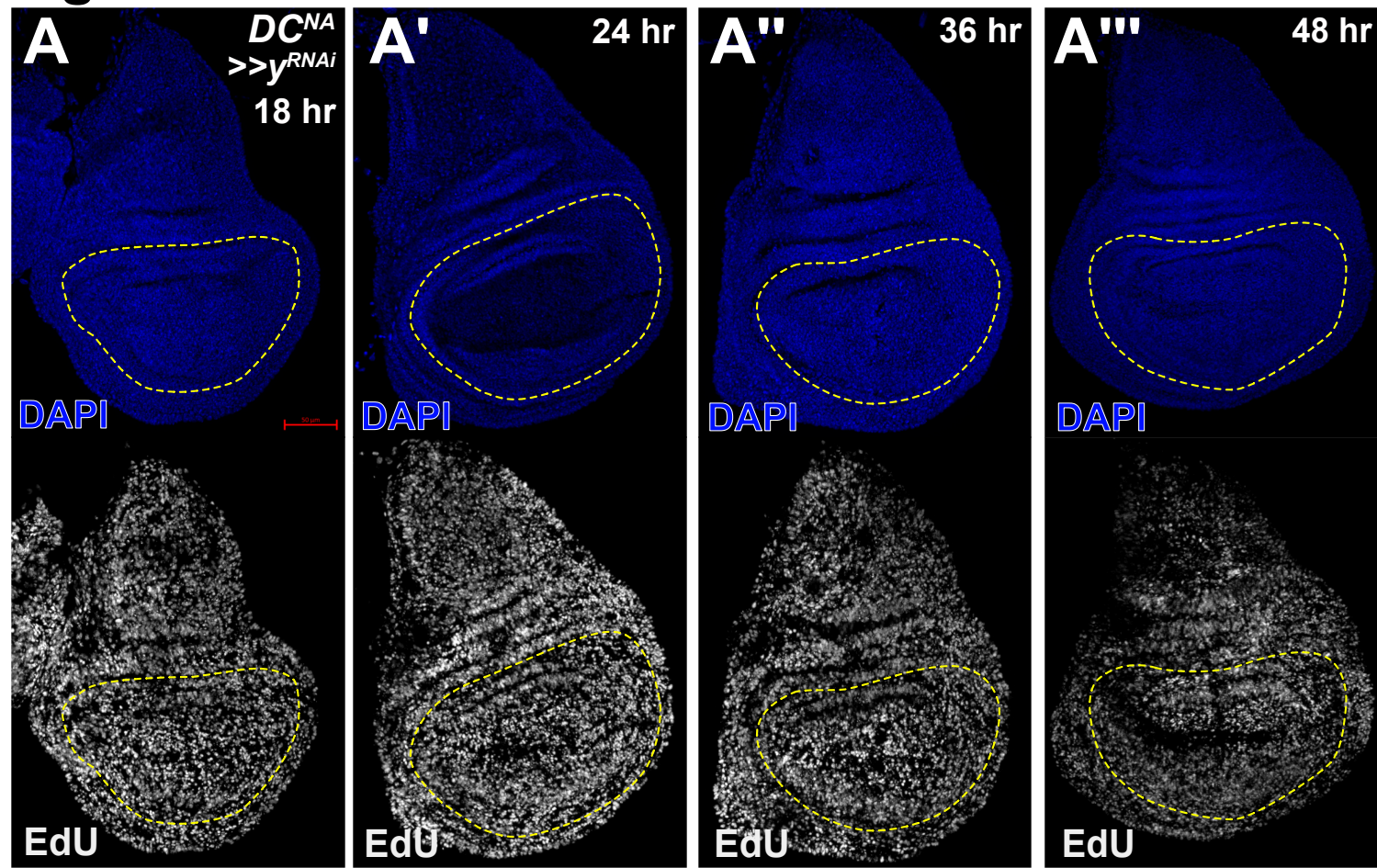


**Figure S3**



**D**

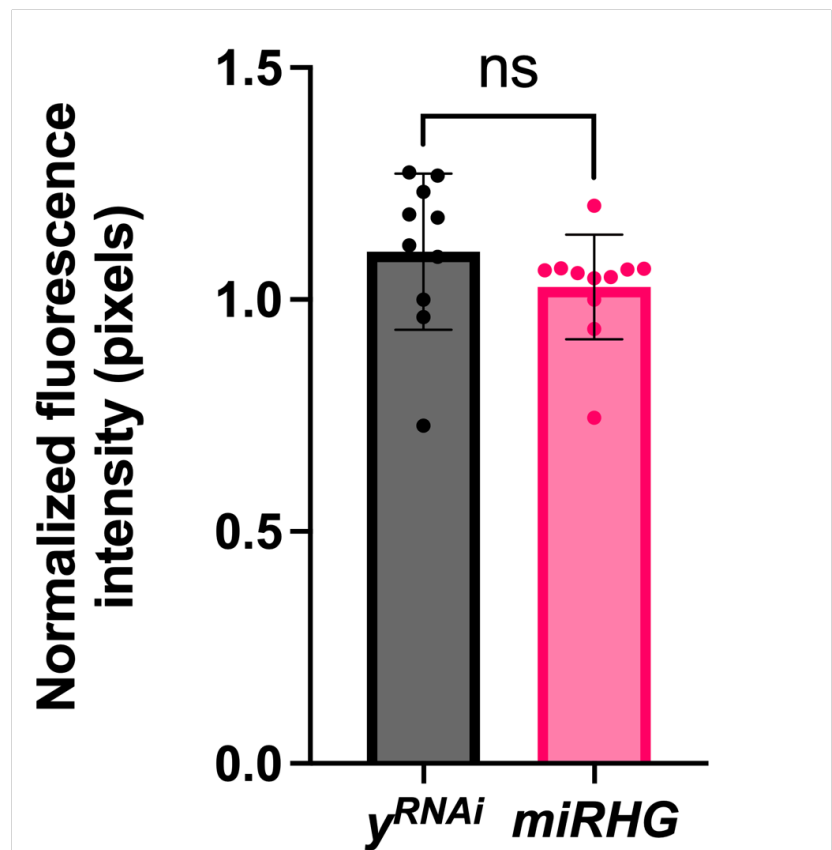


# Figure S4

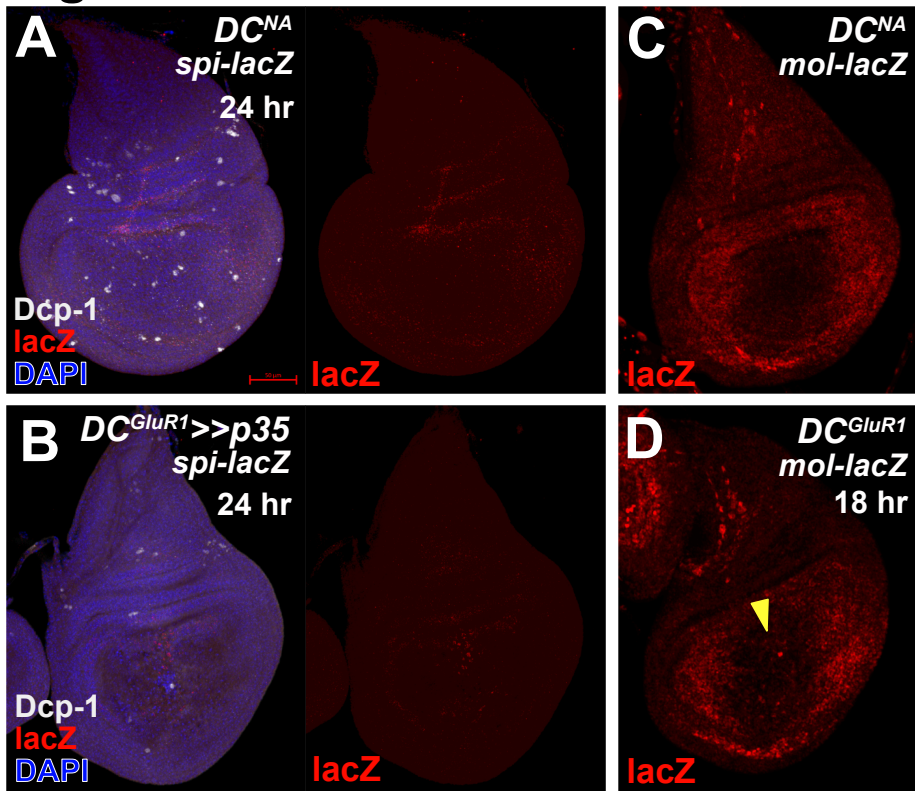


**Figure S5**

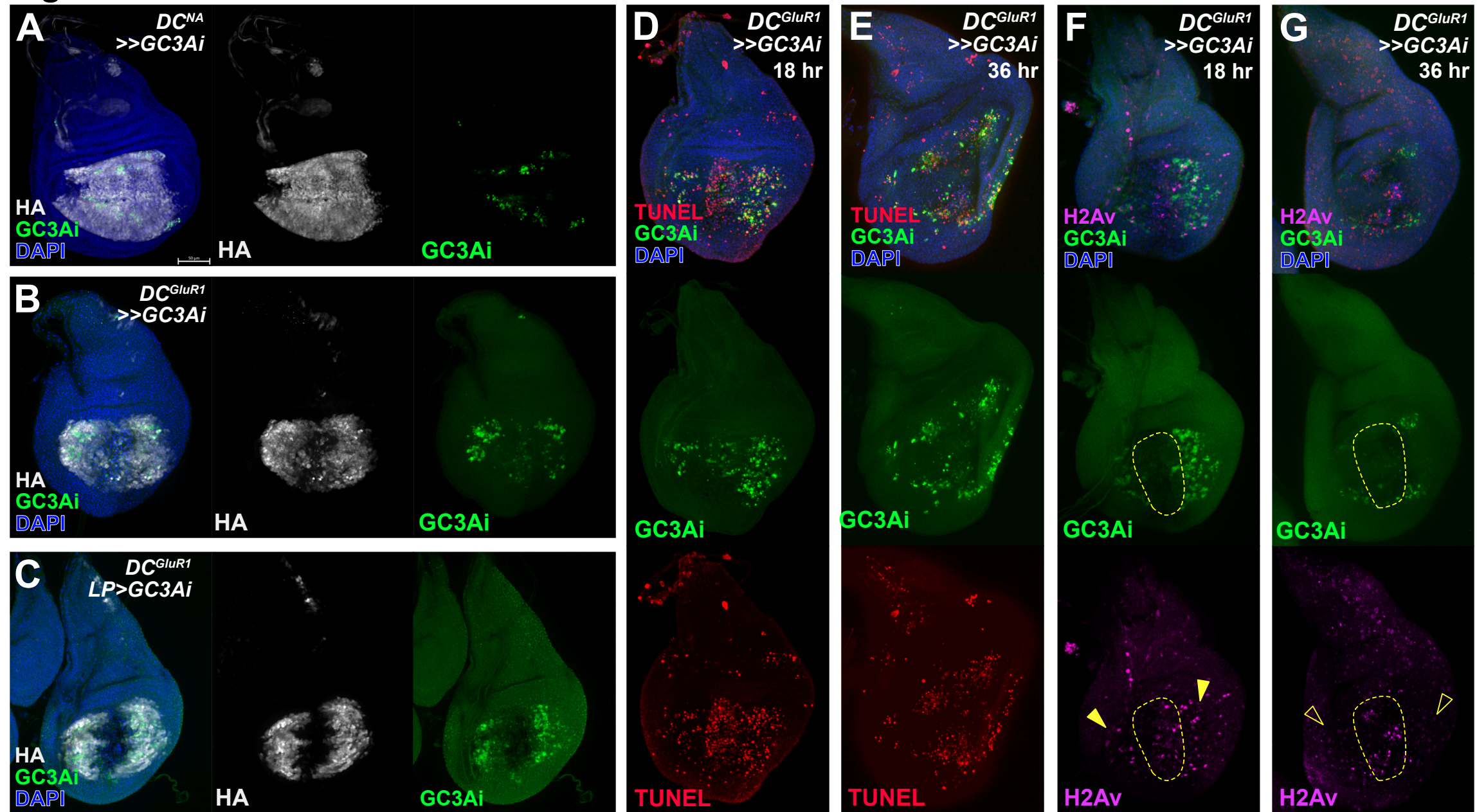


# Figure S6

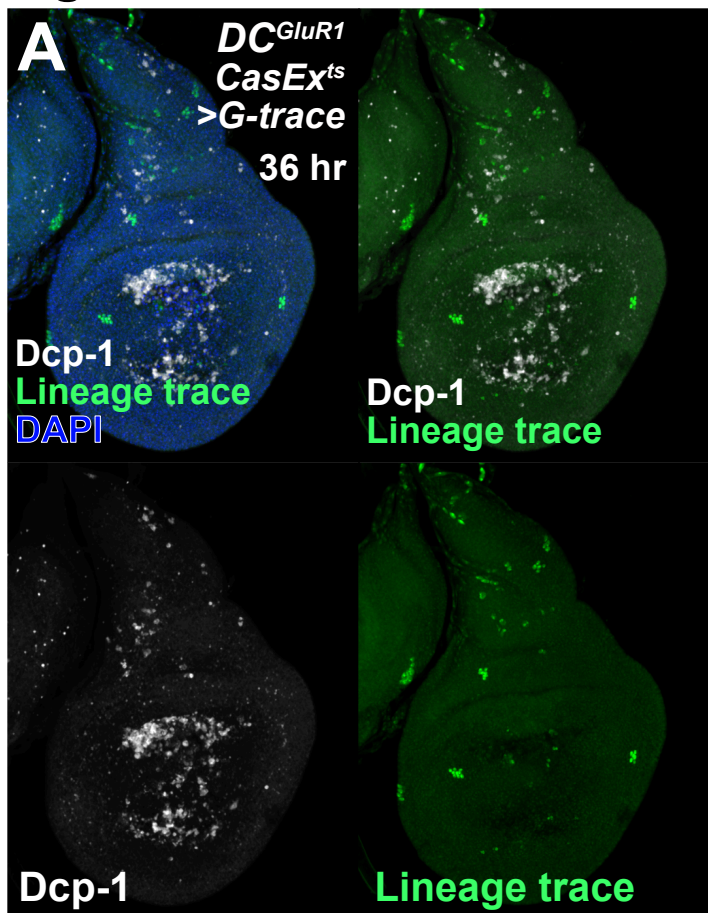


# Figure S7

## A

